Hybrid Polymer-based System for EOR at High Salinity and High Temperature: Experiments

By

Abdulaziz Fattah

in partial fulfillment of the requirements for the degree of

Master of Science

in Applied Earth Sciences

at the Delft University of Technology,

to be defended publicly on Wednesday 12 February 2020 at 09.30 am

Supervisors:	Prof. Dr. Pacelli Zitha	Delft University of Technology
	Ir. Mohsen Mirzaie Yegane	Delft University of Technology

Thesis committee:	Prof. Dr. Pacelli Zitha (Chair)	Delft University of Technology
	Dr. Denis Voscov	Delft University of Technology
	Dr. Pouyan Boukany	Delft University of Technology
	Ir. Mohsen Mirzaie Yegane	Delft University of Technology

Abstract

Polymer flooding plays an essential role in Enhanced Oil Recovery by means of achieving a more favorable mobility ratio through increasing the viscosity of the displacing phase and thus improve macroscopic sweep efficiency. Conventional polymer, e.g., hydrolyzed polyacrylamide, dissolved in brine at high-salinity and high-temperature can be subjected to thermal degradation due to hydrolysis of amide group to acid which can result in precipitation driven by the interaction between acid groups and divalent ions, so these processes lead to loss in viscosifying power of drive fluid, thereby hindering polymer efficiency. To overcome these challenges associated with polymers at harsh conditions, a new hybrid dispersion consists of silica nanoparticles and hydrophobically modified polyacrylamide was proposed. This study aims to investigate the adsorptive and transport behaviour for this novel combination using rheological measurement and core flood experiments. Two-phase experiments were conducted to reveal the potential ability of the dispersion in increasing oil recovery compared to water flooding. Three different systems are used in this study, first, polymer solution at a concentration of 500 mg/L, second, nanofluids containing only SiO_2 particles with a concentration of 5,000 mg/L and the third system is the dispersion of silica nanoparticles at 5,000 mg/L and PAM-98 at 500 mg/L. Rheological tests and single-phase experiment results showed that introducing silica nanoparticles to polymer solution led to the bulk viscosity enhancement and improvement in the adsorptive and transport behaviour of nanofluid. However, two-phase experimental results showed no increase in incremental oil recovery at the given study conditions, since water flooding was highly efficient.

Abdulaziz Fattah
Delft, February 2020

Keywords: Enhanced oil recovery, Polymer flooding, Nanoparticles, Hydrophobically modified polymer, Adsorption, Injectivity, core flood experiments

Acknowledgments

Praise to Almighty for His countless blessings, mercy and protection.

As my thesis comes to an end, I am overwhelmed with great joy in the skills and experiences I gained during this period of time. I acknowledge that this work would not have been done as it is, without the support and involvement of several individuals. Therefore, it would be amiss if the credit would not be given where credit is due.

I am delighted to take this opportunity to thank Mohsen Mirzaie Yegane for his support and encouragement throughout the period of this study. Regular meetings, discussions and feedback helped me to tackle the problem at hand in a more efficient manner. I also owe my gratitude to Prof. Dr. Pacelli Zitha for his support and supervision. I am thankful to him for taking time out of his busy schedule whenever I needed it. His critical comments were extremely helpful.

I would like to thank Michiel Slob from TU Delft's Geoscience & Engineering Laboratory for his help in building the experimental setup and providing technical support throughout the experiments. I also want to extend my gratitude to Dr. Sian Jones for providing excellent technical knowledge during microfluidic experiments and for her advice regarding HSE procedures inside the lab. You always supported me and accepted to be my lab buddy whenever I needed. Further, I would like to thank the remainder of technical staff for their support and encouragement, especially Marc Friebel, for his essential role in setting up the microfluidic experiments.

I want to thank my family for their unconditional love and support ,and thank my friends; special thanks go to my friend Ahmad Tahir who was always there if I needed help.

Finally, no words can be used to describe my gratitude and feelings for my dear wife, for her extreme support and love. I dedicate this work to you as a token of appreciation.

Table of Contents

List of Tables

List of Figures

Nomenclature

C	Concentration [*mg/L, g/mol, g/cm3*]
C^*	Overlap concentration [*mg/L, g/mol, g/ml*]
$\dot{\gamma}$	Shear rate [s^{-1}]
$\dot{\gamma_{C2}}$	Second critical shear rate [s^{-1}]
μ	Viscosity of polymer [*mPa.s*]
μ_0	Zero shear viscosity [*mPa.s*]
μ_∞	Infinite shear viscosity [*mPa.s*]
λ	Relaxation time[s]
τ	Shear stress [Pa]
RF	Resistance factor (-)
RRF	Residual resistant factor (-)
ΔP_p	Differential pressure of polymer injection [*mBar*]
ΔP_{NF}	Differential pressure of nanofluids [*mBar*]
ΔP_b^0	Differential pressure of brine before polymer injection [*mBar*]
ΔP_b^1	Differential pressure of brine after polymer injection [*mBar*]
ΔP_{HS}	Differential pressure of hybrid solution after polymer injection [*mBar*]
λ_i	mobility of injected fluids
λ_o	mobility of the oil phase
Kr_i	Relative permeability of injected fluid [-]
Kr_O	Relative permeability of oil [-]
μ_i	The Viscosity of injected fluid [*mPa. s*]
μ_o	The Viscosity of the oil phase [*mPa. s*]
M	Mobility ratio phase
PH	Hydrogen ions concentration
Wp	Amount of water produced[cm^3]
k_o	Effective permeability of oil
k_{ro}	Relative permeability of oil [-]
μ_o	Viscosity of oil [*mPa.s*]
Wo	Amount of oil produced [cm^3]
S_{oi}	Initial oil saturation [%]
S_{or_wF}	Residual oil saturation to water flooding [%]
R_{f_wf}	Recovery factor to water flooding [%]
k_w	Effective permeability of the water phase [*mD*]
k_{rw}	Relative permeability of the water phase [-]
μ_w	The Viscosity of water phase [*mPa. s*]
λ_w	Mobility of the water phase
$M_{w/o}$	Mobility ratio of water phase to oil phase [-]
T	Temperature [℃]

Abbreviations

PAM-98	Hydrophobically modified polyacrylamide
HPAM	Hydrolyzed Polyacrylamide
PAM	Polyacrylamide
CO_2	Carbon Dioxide
SiO_2	Silica oxide
TDS	Total dissolved solids
RF	Resistance factor
SNPs	Silica nanoparticles

SNFs	Silica nanofluids
RRF	Residual resistance factor
Rf	Recovery factor
O_{IIP}	Oil initially in place
$CaCl_2$	Calcium chloride
Ca^{++}	Calcium ions
PV	Pore Volume
$W_t\,\%$	Weight percent
$NaCl$	Sodium Chloride
$HPAM$	Hydrolyzed Polyacrylamide
PAM	Polyacrylamide
CO_2	Carbon Dioxide
$peek$	Poly-Ether Ether-Ketone
UV	VIS Ultraviolet-visible
TOC	Total Organic Carbon
NPs	Nanoparticles
Na^+	Sodium ions

Subscript

HS	Hybrid solution
o	Oil
i	Initial
w	water
wf	Waterflood
p	polymer

System of units

S	Second
℃	Degree centigrade
ppm	Parts per million
mol	Moles
$g/\,l$	Gram per liter
$g/\,mol$	Gram per mol
$g\,/\,cm^3$	Gram per cubic centimeter
$\mu\ gr$	microgram
g/ml	Gram per milliliter
g	Gram
Kg	kilogram
mD	millidarcy
m	Meter
cm^3	Centimeter cubic

1

Introduction

The motive force behind the development of EOR techniques is a large amount of oil left behind in all kinds of reservoirs after the application of primary and secondary recovery. This is either because oil is trapped by capillary forces or bypassed because of reservoir heterogeneity or due to poor mobility ratio between the aqueous and oleic phase (Sheng, 2014). This substantial amount of oil is necessary to be exploited to meet the increasing demand for energy due to the high population and industrial development (Wang, Liu et al. 2003). Among EOR techniques, polymer flooding, which is a chemical EOR method involves adding high molecular weight water-soluble polymers to the drive fluid, which consequently leads to an increase in the viscosity and improvement of mobility ratio.

Different types of polymers are used to improve sweep efficiency. However, the most effective and widely used polymers are polyacrylamide and partially hydrolyzed polyacrylamide, because they have good water solubility, high resistance to bacterial attack, can be produced in high quantity with low cost and ability to provide good mobility control (Sorbie, 1991). However, some limitations arise with the application of these polymers in some of the oil reservoirs with a harsh environment such as high temperature and high salinity conditions. Polyacrylamide solution used during polymer flooding at high temperatures can undergo partial hydrolysis and a high degree of hydrolysis resulting in changes in solution properties such as stability and viscosity loss. On the other hand, high salinity of water means a significant amount of ions (Ca^{+2}, Na^{+}) interacting with polyelectrolyte and this reduces the repulsive forces between polymer molecules and therefore decreasing the hydrodynamic volume.

In recent years, a lot of attention has been drawn to investigate the capability of silica nanoparticles for EOR applications due to their unique properties resulting from their small dimensions (1 – 100)nm, high specific surface area (Zhang, Nikolov et al. 2014), low cost, environmental friendliness and also the chemical surface of nanoparticles that can be functionalized with different terminal group ranges from hydrophilic to hydrophobic groups (Miranda, Lara et al. 2012).

However, a few experimental studies investigated the potential role of introducing nanoparticles into the polymer to increase the injectant viscosity and improve the final oil recovery. (Maghzi, 2014) investigated the effect of adding silica nanoparticles on the rheological behaviour of polymer at different salinity. He showed that the introduction of SNPs increased the viscosity of PAM and prevented its degradation in the presence of salts. (Hu, 2017) studied the rheological properties of hybrid suspension consists of SNPs and HPAM and it was concluded that inclusion of SiO_2 significantly improved the viscosity and viscoelastic properties of HPAM under high salinity and temperature.

Despite excellent researches on conventional polymer flooding and nanofluids in EOR, there has been scarce works on the application of polymer and silica nanoparticle dispersion to improve the

performance of polymer flooding at high temperatures and high salinity. To our knowledge, no work so far addressed the adsorptive and injectivity behaviour of this novel dispersion in dynamic core flood experiments.

In this study, we are interested in exploring and appraising the adsorptive and transport behaviour of hybrid dispersion at high salinity (200,000 ±1,000) mg/L and high temperature (70 ±1) C° in Bentheimer sandstone and evaluate its efficiency for oil recovery using high viscous oil.

1.1 Statement of problem

The water-soluble polymers are used in EOR to reduce the mobility ratio of injected fluid to the displaced phase by increasing the viscosity of displacing fluid. However, the performance of conventional polymer, e.g., HPAM, can considerably be influenced if applied in hydrocarbon reservoirs with severe conditions of high salinity and temperature (Sorbie 1991). The high salinity/hardness of synthetic brine used to prepare the polymer solution, particularly the divalent cations (Ca^{+2}), reduces the viscosity substantially due to strong binding to the negatively charged carboxylic group. This weakens the electrostatic resistance and makes the polymer chains to coil up that result in reducing the hydrodynamic volume and loss in viscosity. In a hostile environment, it can lead to precipitation (Zaitoun and Potie 1983). As a result of this, the viscosity reduction can only be compensated using a higher amount of the polymer that can make the project inappropriate from an economic point of view. On the other hand, the higher the reservoir temperature is, the less stable the polymer will be since an increase in temperature increases the degree of hydrolysis, and this can accelerate the chemical degradation of the polymer. Therefore, efforts are made to develop a new formulation of Hybrid novel polymer-based system to improve the rheological behaviour of the polymer, and resistance to high salinity and temperature effects (Niu, Jian et al. 2001, Yang, Mao et al. 2019).

1.2 Research objective

The objective of the research is to investigate the behaviour of polymer and nanoparticle systems in the bulk and porous media using viscosity measurements and pressure drop data, besides, quantify their retention in porous media. The tasks of this research are:

1.2.1 Conduct rheological studies in the bulk phase for the polymer (PAM-98) used as a basic component in the hybrid system, model and interpret the rheological behavior.

The polymer solution is prepared using synthetic brine with very high salinity. The total dissolved solids (TDS) of brine is 200,000 ± 1,000 mg/L including 15,000 mg/L of calcium as divalent cation. The polymer solution at different concentrations (500 – 10,000) mg/L is subjected to a range of shear rate (1 - 100) s^{-1}.

1.2.2 Conduct single-phase experiments to investigate the propagation of the systems in porous media

Different solutions are prepared at different concentrations, which are PAM-98 with a concentration of 500 mg/L, nanoparticles with concentration 5,000 mg/L, and finally, a combination of polymer and nanoparticles. The viscosity of each chemical material is measured (see Table 4.9 and Figure 4.9). The

experiments are done to quantify the retention amount for injected dispersions and to evaluate their injectivity through recording pressure data.

1.2.3 Performing two-phase experiments to investigate the ability of the materials to increase sweep efficiency.

Two-phase experiments are performed using water as secondary recovery, and then the hybrid system is injected as a tertiary method, details in (Section 4.3)

2

Background

This chapter discusses fundamental concepts and necessary information about polymer and nanoparticles as chemical materials used for EOR flooding. This includes, the structural properties, polymer rheology, retention of polymer in porous media, and the different retention mechanisms. The main mechanisms responsible for improving oil recovery using nanoparticles are also reviewed in this chapter.

2.1 Polymer characteristics

2.1.1 Hydrophobically modified polymer

Hydrophobically-Modified Polyacrylamide (HMPAM) are polymers that contain a small number of hydrophobic groups attached directly to the hydrophilic polymer backbone. The molar incorporation rate of the hydrophobic groups should be minimized to ensure the water solubility of the polymer. The aggregation of hydrophobic groups in aqueous solution depending on the polymer concentration may form a network structure, generally resulting in microdomains formation, as illustrated in Figure 2.1, and this causes the increase in viscosity (Argillier, Audibert et al. 1996, Yang, Mao et al. 2019). Shear application in conventional pseudoplastic polymeric solution reduces the viscosity, due to disruption in the hydrophobic association.

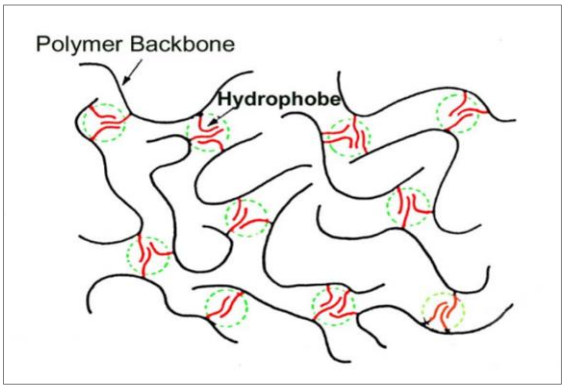

Figure 2.1. Representation of interactions of hydrophobes in the hydrophobically modified polymer (Taylor and Nasr-El-Din 2007)

2.1.2 Concentration regime

To provide a further understanding of rheological behavior, the relation between the concentration and the conformation should be introduced through what is called conformation of polymer in the solvent and concentration regime.

Although the polymer molecules consist of long chains and each chain has many monomers, they will not be fully extended in straight morphology. Instead, they tend to adopt a coiled-like shape as it can be seen in Figure 2.2**.** The radius of these small spheres is called the radius of gyration. Based on polymer concentration, the polymer solution can be classified as dilute, semi-dilute, and concentrated regimes (Wang, Li et al. 2010, Yerramilli 2012).

a- Dilute system: The concentration of polymer *C* is less than the threshold concentration $C^{\star}$, known as overlapped concentration. The polymer molecules act independently, and they do not interact with each other, rather they do interact essentially with brine molecules. The intramolecular hydrophobic association within the polymer dominates the behaviour of the polymer and may reduce the hydrodynamic volume.

a- Semi-dilute system: As the concentration of polymer increases, the distance between the coils decreases, and when the critical overlap concentration $C^{\star}$, is reached, the coils can be deformed and closely packed, and polymer chains interact with each other. Above $C^{\star}$, the interactions between entangled chain molecules dominates. The chains behave like a transient network, which substantially increases the viscosity of the solution. The solution viscosity increases faster with increasing polymer concentration compared to the dilute regime.

b- Concentrated regime: When the number of polymer molecules per unit volume increases to high value, then the concentration of the polymer molecules will exceed the second threshold, i.e., $C \gg C^{*}$, subsequently, the coils become densely packed and entangled. The interaction between polymer chains becomes stronger as polymer concentration increases. The solution viscosity in this regime will be higher than in the semi dilute regime. The intermolecular associations between polymers become more dominant, and hydrodynamic volume will increase.

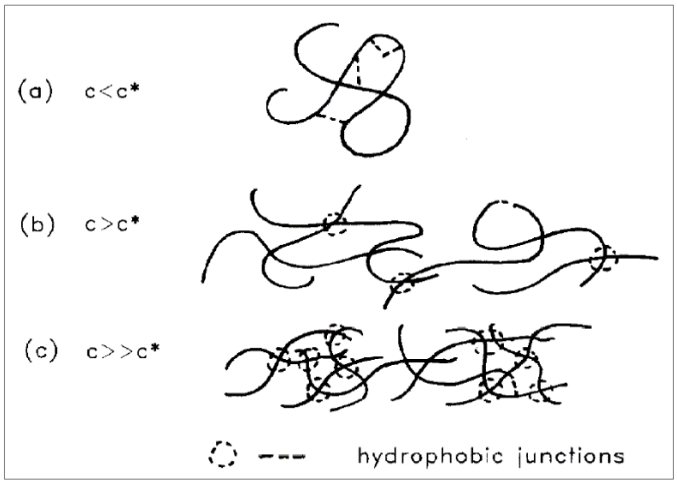

Figure 2.2. Schematic illustration for the possible state of chain association in (a) dilute regime, (b) the semi dilute regime and (c) the concentrated regime, from (Aubry and Moan 1998)

2.1.3 Polymer rheology in bulk and porous media

Polymer solution used in EOR is considered to be non-Newtonian fluid in which the viscosity of polymer solution depends on both polymer concentration and shear rate. Studying the flow behaviour of this type of fluid is known as rheology. The study of the rheological behaviour of polymers prior to injecting in the field is very important to understand how this material behaves in both bulk and porous media. The viscosity of the polymer measured in bulk using a rheometer is known as shear viscosity. While apparent (in situ) viscosity refers to the polymer viscosity in porous media.

Since mid-1960's different polymers were used for EOR application. However, they can generally be categorized into two main types; biopolymer and synthetic polymers (Sorbie 1991). These polymers might have similar shear viscosity when measured using a rheometer, but they might have different in situ rheological behaviour in reservoir formation. It is worth mentioning that in a low and intermediate-range of shear rate, both shear and apparent viscosity show the same trend. Still, at high values of shear rate, the behaviour is differentiated. The difference in behaviour is illustrated in Figure 2.3. This behaviour is often seen in the complex geometry of pores and molecular structure. Biopolymers exhibit essentially a shear-thinning behaviour due to their semi-rigid rodlike structure, which does not allow extensional flow, whereas viscoelastic synthetic polymers have a flexible structure. Hence, they can behave both shear-thinning and flow thickening behaviour (Sheng 2010).

(a) (b)

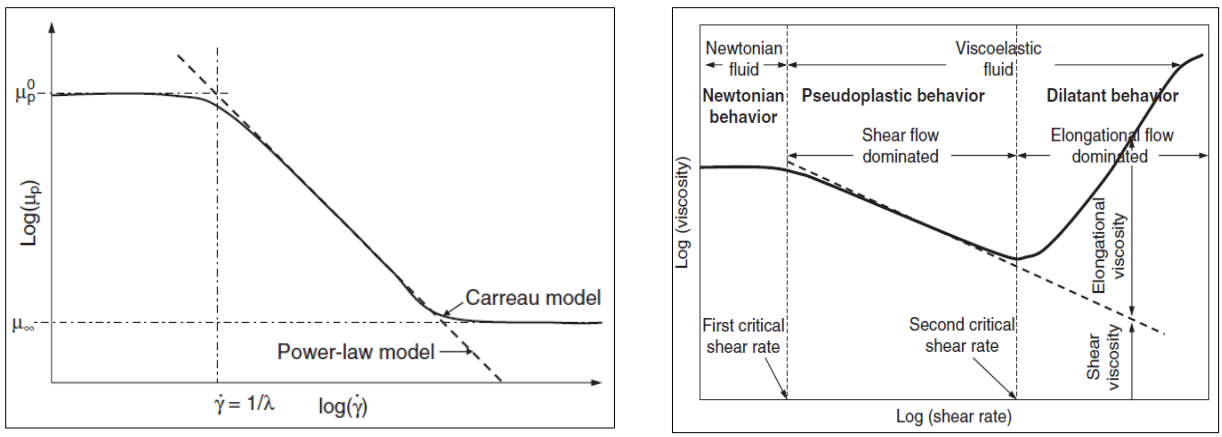

Figure 2.3. Schematic description of polymer behaviour in (a) only Bulk, where a comparison between power low model and Carreau model is made and (b) viscoelastic polymer in bulk and porous media, from (Sheng 2010)

Newtonian behavior, i.e. where viscosity is independent of the imposed shear rate can be noticed if the applied shear rate is lower than the first critical $\gamma < \dot{\gamma_{C1}}$. As the shear rate increases further, in situ viscosity decreases, and polymer solution exhibits shear-thinning behavior. During shear thinning, with increasing shear rates, polymer molecules start to disentangle until viscosity approaching another Newtonian plateau, where disentanglement reaches the high value.

Above the second critical shear rate $\dot{\gamma_{C2}}$, owing to the flexible polymers chains, the extensional flow becomes predominant. The geometry of pores and grains of porous media along with injected fluid can generate different stress fields as polymer flows in the rock. The exerted forces from complicated converging-diverging geometry cause polymer stretch and contract, and therefore polymer chains

have insufficient time to recoil and align with flow direction(Zitha, Chauveteau et al. 2001). Coil stretching and alignment with flow enhance the frictional forces between elongated chains and solvent and result in extra energy dissipation (Jouenne and Heurteux 2017). This will cause pressure build-up and high apparent viscosity. If the stretch rates that are associated with shear-thickening are high enough, chain stretch might evolve into chain fragmentation and eventually yielding mechanical degradation that can, in turn, lead to apparent viscosity loss (Al-Shakry, Skauge et al. 2018)

Viscosity correlations

The viscosity is the primary parameter influence the rheological behaviour of polymer solution. For non-Newtonian fluid, the viscosity represents the ratio of shear stress to shear rate, with viscosity being also function of shear rate.

$$\tau = -\mu(\dot{\gamma})\frac{dv}{dr} = \mu(\dot{\gamma}) \times \dot{\gamma} \qquad \text{Eq.2.1}$$

where $\dot{\gamma}$ is the shear rate, τ the shear stress, and η is the apparent viscosity. Several correlations are proposed to find the relation between the viscosity and shear rate. The simplest model is the power-law model, which is sometimes called the law of Ostwald and de Waele (Sorbie 1991).

$$\tau = -\mu(\dot{\gamma}) = K \times \dot{\gamma}^{n-1} \qquad \text{Eq.2.2}$$

here *K* and *n* are constants. The value of the power-law exponent for non-Newtonian fluid is $0 < n < 1$, and for Newtonian fluid is $n=1$. As can be shown in Figure 2.3, the equation Eq.2.2 is only valid for the shear-thinning (Pseudoplastic) region. For a better description of rheological behavior, the region of low and higher shear rate must be incorporated, and thus a more satisfactory model needs to be used. The Carreau-Yasuda model (Carreau,1972); Eq.2.3 is adopted in this study to model the bulk viscosity as it will be seen in (section 5.1)

$$\mu = \mu_\infty + (\mu_0 - \mu_\infty)[1 + (\lambda\dot{\gamma})^a]^{(\frac{n-1}{a})} \qquad \text{Eq.2.3}$$

where μ_0 is the viscosity at zero shear rate, μ_∞ infinite shear viscosity, λ is time empirical constant (relaxation time) and *n* is the same as power-law index, a determines the transition between low shear rate and power-law model (Sorbie 1991). The parameters n, λ, a can be found by fitting the experimental data and Carreau-Yasuda model.

2.1.4 Polymer retention

The objective of adding water-soluble polymers is to increase the viscosity of injected brine. However, significant interactions between transported polymer molecules and rock surface of the reservoir take place. These interactions might remove some of the polymer molecules and create a polymer bank wholly or partially denuded from the polymer molecules. The possible mechanisms of polymer retention are shown in Figure 2.4

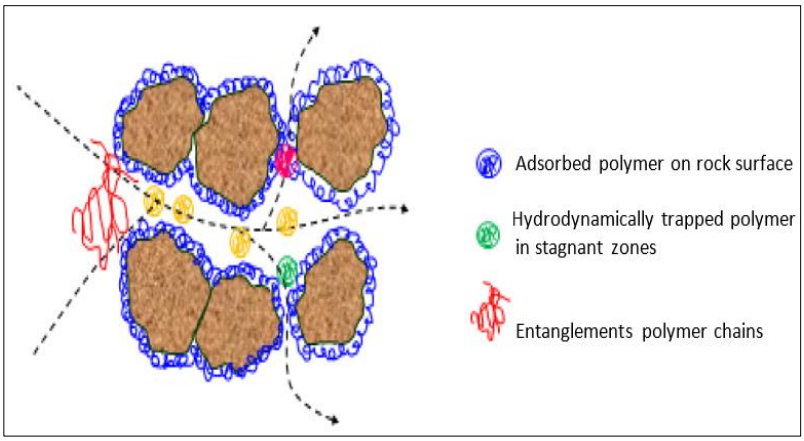

Figure 2.4. Schematic of polymer retention mechanisms in porous media (from Yerramilli, 2012)

First, mechanical entrapment can happen when polymer molecules entre small pores with average pores through diameter relatively smaller than the size of polymer molecules. Small molecules of an aqueous phase and dissolved salts can pass, but large polymer molecules will be trapped and accumulated at the inlet of tiny pores. They can increase local polymer concentration to value higher than the injected concentration(Szabo 1975). The potential consequence of this type of retention is permanent damage to the reservoir and injectivity loss due to partially blocked polymer path flow.

The second mechanism for retention is hydrodynamic retention, which is associated with the flow rate of injectant. This means that although the amount of retained polymer can reach steady-state after injecting several pore volumes, a sudden increase in flow rate will cause extra polymer loss. However, hydrodynamic retention is believed to be irreversible, i.e., part of retained polymer molecules can be released and join the main flow stream when the flow rate is adjusted(Chauveteau and Kohler 1974).

Adsorption is yet another and one of the key retention mechanisms in porous media. Polymers used in EOR have relatively high molecular weights, long chains and contain many polar groups distributed along the extended chain. Many of these polar groups will attach to different polar points on the rock surface due to physical interactions, such as Van der Waals forces or hydrogen bonding, causing the polymer to be retained. In practice, adsorption is considered to be irreversible (Sorbie 1991, Green and Willhite 1998). Although one polar group may detach from the rock surface, another point of the chain will remain in place. Statistically, it is unlikely that the polymer molecules would release all the attached points at the same time, and the amount of the polymer adsorption is proportional to the accessible surface area to polymer molecules.

“Bridging adsorption” (Zitha, Chauveteau et al. 2001), is a mechanism proposed to explain the unsteady-state flow for flexible polymer at a high-velocity gradient. Flexible polymer molecules can be stretched significantly in the elongational flow field. Because of a series of contractions and extensions in porous media, the stretched molecules will not have enough time to relax. Adsorption of elongated molecules so that they bridge over pore increase the flow resistance substantially.

Polymer retention has significant effects on polymer propagation, which is governed by accessible pore volume and retention. Since porous media has complex structures and different pore sizes, it is fair to envisage that large molecules of the polymer will not be able to penetrate in all pore space, but it will be accessible to solvent molecules. Therefore, this inaccessible pore volume will accelerate the

polymer flow (Dawson and Lantz 1972). In contrast, retention can delay polymer propagation through porous media and consequently delay oil displacement and oil recovery. Polymer retention can cause a reduction in the original rock permeability and viscosity loss, which in turn lowers the macroscopic efficiency.

Factors that influence the retention of polymers in porous medium include polymer type and concentration, molecular weight, rock permeability, flow rate, salinity, temperature, and the presence of clay minerals. Overall, polymer retention is an important factor that governs the economic viability of a polymer flooding process as they have an impact on the rock permeability, the viscosity of the injected polymer solution, and consequently, the oil recovery process.

In this study, retention is evaluated by effluents analysis and using experimental pressure drop to calculate resistance factor (*RF*), which is a measurement of mobility reduction (Eq.2.4) and a residual resistance factor (*RRF*), which is a measurement of permeability reduction (Eq.2.5). The results are shown in Chapter 4.2.

$$RF = \frac{\Delta P_p}{\Delta P_b^0} \qquad \text{Eq.2.4}$$

ΔP_p: differential pressure of polymer injection

ΔP_b^0: differential pressure of brine injection before polymer injection

$$RRF = \frac{\Delta P_b^1}{\Delta P_b^0} \qquad \text{Eq.2.5}$$

ΔP_b^1: differential pressure of brine injection after the polymer injection

ΔP_b^0: differential pressure of brine injection before polymer injection

2.2 Nanoparticles for EOR

In this Subsection, the main mechanisms responsible for improving oil recovery using nanoparticles are discussed including mobility control and wettability alteration.

2.2.1 Nanoparticles for mobility control

To enhance oil recovery from an exploited reservoir, controlling the mobility ratio is an important parameter. The mobility ratio is given by equation (1):

$$M = \frac{\lambda_i}{\lambda_o} = \frac{Kr_i/\mu_i}{Kr_O/\mu_o} = \frac{Kr_i.\mu_o}{Kr_o\,\mu_i} \qquad \text{Eq.2.6}$$

where $\lambda_{i,}$ λ_o are the mobility of injected fluids and displaced oil, respectively. kr_i and kr_O are the relative permeability of the injected fluid and oil; μ_i , μ_o are the viscosity of injected fluids and oil.

Eq.2.6, shows that the mobility can be decreased either by viscosity enhancement of injected fluids or reducing the oil viscosity. Measuring the viscosity of nanofluid is important since it indicates the fluid's resistance to flow. On the other hand, many factors affect the viscosity of nanofluids such as base fluid type, temperature, particles size, particles concentration and particles aggregation. An experimental investigation was conducted by (Jamshidi and Khodadadi 2012) to study the effects of adding silica

nanoparticles on the viscosity of the base fluid where different particle volume fraction was used (0.02 – 0.1) vol%. It was shown that the viscosity of the suspension is enhanced with nanoparticles and viscosity increases exponentially with an increasing volume fraction of nanoparticles due to the direct effect of nanoparticles on the internal viscous shear stresses. They also showed that increasing temperature reduces viscosity because of reduction in inter- particles/inter-molecular forces.

2.2.2 Nanoparticles for surface wettability alteration

- **Disjoining pressure**

The NPs in the dispersion tends to form a self-assembled wedge film when they come into contact with a discontinuous phase. Confinement of the thin film contains small particles between an oil drop and rock surface, and their arrangement in ordered layers increases the entropy of the system, permitting a higher degree of freedom for the nanoparticles in the bulk liquid. This arrangement exerts excess pressure in the film relative to the bulk and creates what is called disjoining pressure. Disjoining pressure is the pressure required to oppose the fluid/rock attractive forces and represent the net pressure difference between the pressure in the thin film and bulk pressure (Chengara, Nikolov et al. 2004). The origin of the disjoining pressure is integral of Brownian motion, electrostatic repulsion between the particles, and structural ordering of the nanoparticles (Churaev 2003). The significant role of disjoining pressure is to enhance the wetting and spreading of nanofluids on the rock surface compared to the base fluid without the particles.

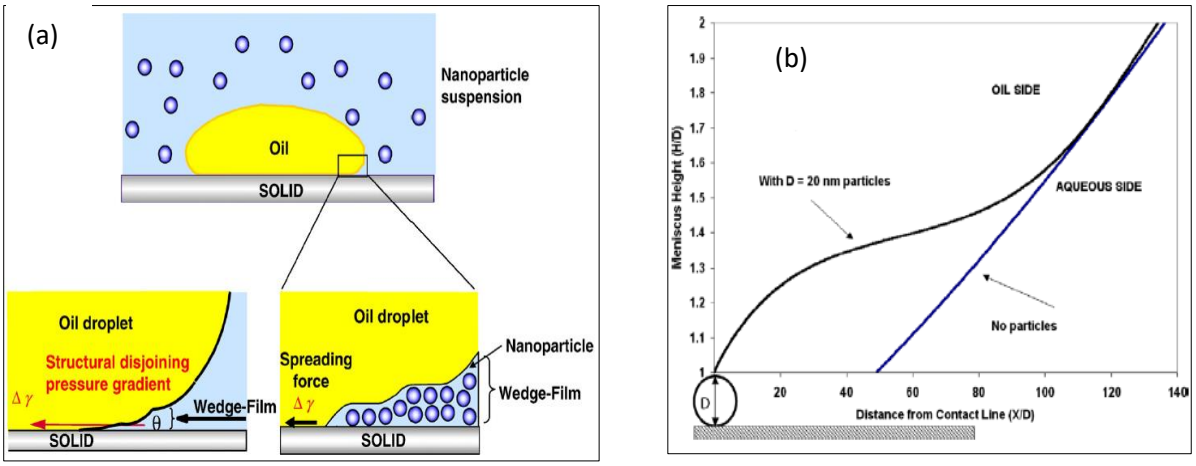

Figure 2.5. Left (a) shows the arrangement of nanoparticles in the wedge film resulting in a disjoining pressure gradient at the wedge vortex (Kondiparty, Nikolov et al. 2012). Right (b) shows the shape of miscues profile in the wedge in the presence and absence of nanoparticles (Chengara, Nikolov et al. 2004).

- **Wettability modification**

Formation wettability is a very important characteristic for many types of oil recovery methods, and it refers to the tendency of one fluid to spread on or adhere to a solid surface in the presence of another immiscible fluid. Wettability has an impact on other reservoir parameters when multi-phase experiments are conducted, such as relative permeability, distribution of residual oil saturation, and oil recovery efficiency (Craig 1971). Measuring the reservoir wettability before and after applying any

EOR technique, including nanofluid, is one of the key aspects which can assist the researchers in determining the potential mechanisms leading to the incremental oil production during the laboratory flood, if any improvement is made. There are different approaches available for wettability measurement in the literature, including quantitative and qualitative methods(Anderson 1986). Contact angle measurement is one of the quantitative methods adopted by many studies to evaluate the performance of silica-based nanofluid in improving oil recovery from sandstone reservoirs. Laboratory core plug experiments conducted by (Roustaei, Saffarzadeh et al. 2013) to investigate the effectiveness of modified nano-silica in the oil recovery using light and intermediate oil reservoirs. They estimated the wettability conditions before and after the surface treatment with nanoparticles by measuring the oil phase contact angle. The results of the measurements showed a rock wettability alteration. However, interfacial tension and wettability reduction were more pronounced for light oil, and they concluded that these two processes are responsible for oil recovery enhancement. Another study done by (Hendraningrat and Torsæter 2014) evaluates the impact of initial rock wettability and silica nanofluid post-flush on the oil recovery. The core floods experiments performed at different temperatures (20, 50, 80) C°. The results showed that injecting silica oxide (Si2O) as tertiary recovery caused higher pressure to drop over the core and yields additional oil recovery. To find possible displacement mechanisms, they also measured the contact angle and IFT as a way to characterize the wettability alteration. They came to the same conclusion as the previous study that wettability alteration can be a possible displacement mechanism.

2.2.3 Transport of nanoparticles in porous media

For nanosized particles to increase oil sweep efficiency, they must be able to travel deep into the reservoir. Several studies reported few challenges accompanied by the flow of nanoparticles in porous media. Therefore, it is essential to understand the mechanisms that affect the flow of NPs. There are primarily three mechanisms affecting the transport of nanoparticles:

- **Nanoparticle filtration**

Filtration occurs when the size of particles is larger than some of the pores in the porous media. This may even happen for non-aggregated nanoparticles when injected in very low permeability rocks. Therefore, the size and shape of the nanoparticles are important parameters that can affect filtration. Particle size distribution is important since filtration can be initiated by the larger particles, which in turn can cause further filtration due to a decrease in pore size because of initial filtration (Baez, Ruiz et al. 2012). This problem is encountered in this report during the adsorption test of nano-silica fluid with concentration 5,000 mg/L (Figure 4.7)

- **Stability of NPs:**

After preparing the nanofluids with the desired concentration, it is important to examine the samples before conducting the core experiment to ensure that no precipitation of particles occurs. However, in the presence of high salinity, poor stability may lead to agglomeration and precipitation due to the attractive force enhancement. (Ersenkal, Ziylan et al. 2011) investigated the size of coated iron particles in static and dynamic conditions. They found that the size of particles appeared to be a function of nanoparticle solution concentration in the dynamic test but not in a static test. They hypothesized that forces and torques acting on nanoparticles in the dynamic test could be significant in convergence area and that favors nanoparticle aggregation and filtration. This highlights the

complexity of the effects of dynamic factors (e.g., flow rate) on the effective size of nanoparticles and questions the validity of static measurement to determine the stability under dynamic conditions (Bradford and Torkzaban 2008). In short, static stability does not necessarily mean dynamic stability since the size of particles can be different due to dynamic conditions.

- **Nanoparticles adsorption in porous media**

Adsorption and desorption of nanoparticles can occur even when nanoparticles are having the right size and are stable in solution based on the attraction and repulsion forces between nanoparticles and the surface of porous media. Adsorption can impede the transportation of nanoparticles and should be minimized to improve the injectivity and economics of EOR.

3

Experiment

In this chapter, the main experimental setup components are presented, with an illustrative schematic diagram. In addition, the chemical materials, preparation methods along with experimental procedures are further reported.

3.1 Chemical materials

Different chemicals are used to conduct single-phase experiments, including PAM98, NaCl, CaCl2.2H2O, and silica nanoparticles. Polyacrylamide PAM98 is provided in aqueous solution form at a concentration of 50,000 mg/L, which can be diluted further using demineralized water and brine to any desired concentration. The polymer consists of 98 mol% acrylamide and 2 mol% of t-Butyl-AA, and molecular weight of 3.5 million Dalton(g/mol). Sodium chloride (NaCl, ≥ 99 % purity from Merck), and calcium chloride dihydrate (CaCl2.2H2O, ≥99% from Aldrich) is used for brine preparation. The required amount of both salts depends on the desired salinity and hardness (total salinity is of 200,000 ± 1,000 mg/L, including 15,000 mg/L Ca^{+2}). Potassium iodide (KI) with a concentration of 10,000 mg/L is used as a tracer. Similar materials are used in the two-phase experiment with the addition of oleic to model the reservoir conditions: n-Hexadecane and Ondina Shell oil (see Table 3.1).

Table 3.1. Properties of oil model used in two-phase experiments. The density of n-hexadecane is given at 20 C° [34] and the density of Ondina shell oil is given at 15 C°[35]

properties	n-Hexadecane	Ondina Shell Oil 933
Viscosity (mPa.s) at 25 C°	2.83 ± 0.03	142.82 ± 0.03
Density (g/cm^3)	0.77 ± 0.03	0.879 ± 0.08

3.2 Material preparation

Chemical materials are prepared to meet required specifications such as salinity and concentration, at which the solution or dispersion will be tested. In general, the total salinity of injected materials is kept constant 200,000 ± 1,000 mg/L, while chemicals concentration were assigned differently for each test. In Test 1, polymer concentration was 500 mg/L, while nanofluid had SiO_2 concentration of 5,000 mg/L in Test 2, and hybrid dispersion used in Test 3 had a polymer concentration of 500 mg/L and 5,000 mg/L of nanoparticles.

Brine was prepared by dissolving the required weight of NaCl and $CaCl_2.2H_2O$ in demineralized water on the mass-balance basis and is stirred using a magnetic stirrer for 30 ± 5 min until all solid particles were completely dissolved in water. Measured density and viscosity of synthetic brine at 25 C° were 1.2 ± 0.01 g/cm^3, 1.4 ± 0.01 mPa.s, respectively. Hydrophobically modified silica nanoparticles were also provided as an aqueous suspension at an initial concentration of 281,000 mg/L. The polymer with initial concentration 50,000 mg/L was diluted to concentration 10,000 mg/L in demineralized water and stirred for 24 ± 1 hour. The sample was visually inspected, and once all polymer was dissolved in water, the solution was further diluted to the desired concentration with pre-prepared saline brine and stirred again for about two hours to homogenize the solution. The nanofluid is diluted in a similar way as a polymer solution. The solution of polymer and/or nanoparticles fluid is stirred until the creation of a vortex, and then 10,000 mg/L of potassium iodide (KI) is added. All types of solutions were stirred enough to obtain a homogeneous solution and vacuumed to remove dissolved air. This prevents the oxidation of the dissolved compounds and helps achieving the 100% brine saturation.

3.3 Porous media

The experiments were performed using Cylindrical Bentheimer sandstone cores with the properties presented in Table 3.2 and Table 3.3. Bentheimer sandstone is a shallow marine formation deposited during the Lower Cretaceous, homogeneous, and has relatively constant grain size distribution. It is easy to obtain with low cost from outcrop and contains more than 91% quartz (Peksa, Wolf et al. 2015). Bentheimer has been often used as a model sandstone for laboratory studies. It retains essential reservoir rock characteristics and reproduction and comparison can be done easily due to lateral continuity and homogeneous block scale nature. The cores were drilled and then placed in the oven at 45 ± 1 C° for 48 hours so that they could dry. The cores cast into a thin Epoxy resin layer to guarantee a good adhesion to the next thick layer of the resin and to minimize the amount of glue that can be absorbed into the core reducing the area available for fluid flow. The penetration depth of the glue is approximately 1.0 mm. After an initial layer of resin has dried for 24 hours, the surface of the core is smoothed so the annular space between the mold and the core is filled with degassed glue gradually. The diameter of the core with encased mold should be less than the diameter of the core holder, where space can be filled with brine during the experiment to exert confining pressure. Permeability of the core is calculated for each experiment after sufficient brine saturation using Darcy's law, and pressure drops result from variated flow rates.

Table 3.2. Properties of Bentheimer sandstone used to conduct experimental core flooding. Three different experiments were performed: Test 1 – Single-phase experiment using polymer solution at a concentration of 500 mg/L, Test 2 – Single-phase experiment using silica nanoparticles at concentration 5,000 mg/L, Test 3 – Single-phase experiment using Hybrid solution, all these works are done at constant pressure 25 bar

	Test1	**Test2**	**Test 3**
Porosity (%)	25.0 ± 2.0	25.0 ± 2.0	25.0 ± 2.0
Permeability (mD)	2650.6 ± 161.6	2550.2 ± 152.0	2679.2 ± 165.0
Length (cm)	38.1± 0.1	38.1 ± 0.10	38.1 ± 0.1
Diameter (cm)	3.8 ± 0.1	3.8 ± 0.10	3.8 ± 0.1
Pore Volume (cm^3)	108.0 ± 7.0	108.0 ± 7.0	108.0 ± 7.0

Table 3.3. Properties of Bentheimer sandstone used to conduct two-phase experimental core flooding. Three different experiments were performed: Test 4 – N-hexadecane2, Test 5 – Ondina1, Test 6 – Ondina (3,4)

	Test 4	3- **Test 5**	**4- Test (6,7)**
Porosity (%)	25.0 ± 2.0	25.0 ± 2.0	25.0 ± 2.0
Permeability (mD)	2658.4 ± 164.0	2831.4 ± 175.0	3037.3 ± 188.0
Length (cm)	38.0 ± 0.1	38.0 ± 0.1	38.0 ± 0.1
Diameter (cm)	3.80 ± 0.1	3.80 ± 0.1	3.80 ± 0.1
Pore Volume (cm^3)	108.00 ± 7.0	108.00 ± 7.0	108.00 ± 7.0

3.4 Experimental setup

Figure 3.1 shows a schematic of the experimental setup used to conduct the core flood experiments. The set up consists of a coreholder made of Polyether Ether-Ketone (PEEK) with the Bentheimer core sample. PEEK is a special plastic material with excellent mechanical properties, high transition temperature, good chemical tolerance and transparency to x-rays. The latter property is critical for CT scanning of the cores. The coreholder consists of a cylindrical body with two end-caps at the inlet and the outlet. Holes drilled in a row regular interval along the core length (pressure points) are used for local pressure measurement. A hole drilled opposite to the pressure ports is used to apply a confining pressure which was set equal to the inlet pressure to protect the core from breaking down under differential pressures. The core holder is in line with a dual cylinder pump (Quizix QX_6,000 HC), and they are connected through an inlet line that has two parts: a transparent part and a coiled metal part to ensure proper heating of the injected fluid. A displacement pump provides an accurate flow rate under constant pressure and is used to inject brine and polymer solutions. The pump has a flow rate accuracy of ± 0.02 % about the set point. The maximum pressure for the pump is 100 bar. In two-phase experiments, an additional single-cylinder syringe pump (ISCO type) is used to inject the oil phase. Seven differential pressure transducers (Endress+Hauser type) were used to measure the pressure drop along with the core sample, and two absolute pressure transducers to monitor the inlet and outlet pressure. A back-up pressure is placed at the outlet process line and connected to a gas source; Nitrogen cylinder 100 ± 2 bar, via a pressure regulator valve (Swagelok), to maintain the desired experimental pressure 25 ± 0.5 bar. A fraction collector (GE AKTA Frac-920) is utilized to collect a fixed volume of the effluents for further analysis by setting a specific fraction time. Since all the experiments are required to be conducted at high temperature, the core holder is kept in the oven, where the temperature is fixed at 70.0 ± 0.1°C, and the injected fluid flows through a coiled tube to ensure the solutions are heated up to the desired temperature before entering the core. Experimental data; the pressure drops values from different sections of the core, absolute inlet/outlet pressures, ambient and oven temperature are recorded with a temporal interval equal to 10 sec by a data acquisition system (National Instruments, LabVIEW software). During one phase experiments, the core holder was placed in a vertical position that can unify gravity forces across the core and enhance flow stability, whereas it is fixed in a horizontal position for two-phase experiments.

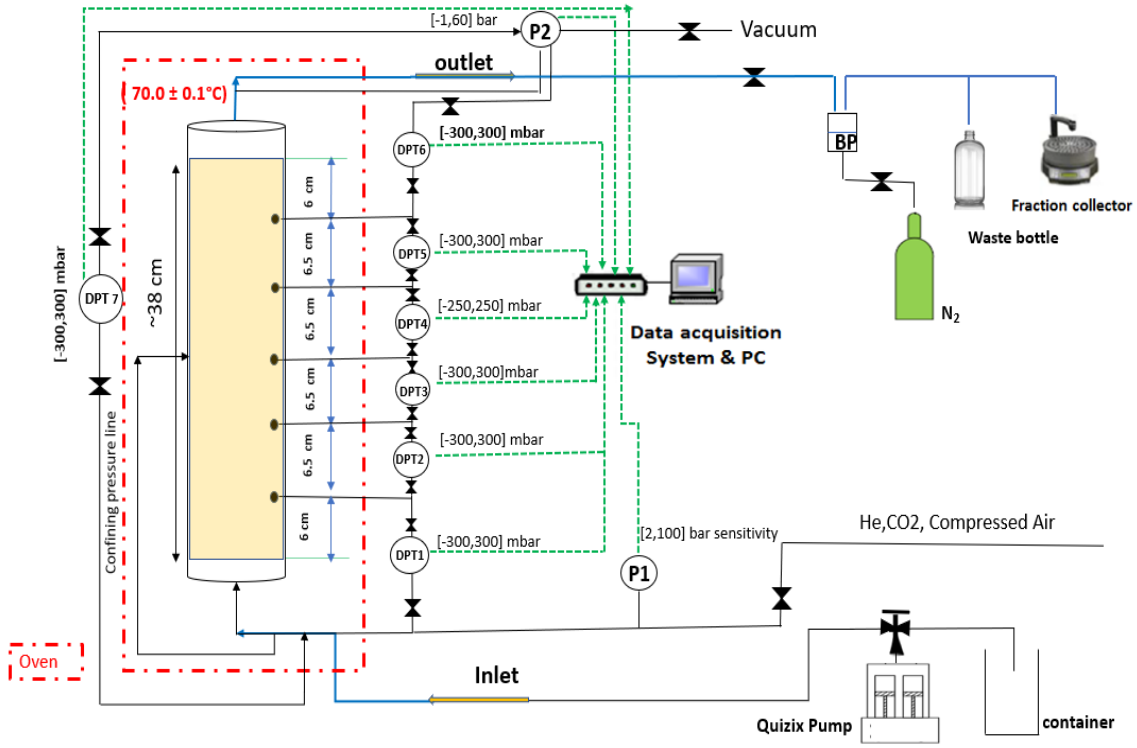

Figure 3.1. Schematic diagram of core flood experimental setup

3.5 Experimental procedures

3.5.1 Rheological measurements in the bulk phase

Prior to conducting any experiment, the rheological test (viscosity) is carried out using a rheometer MCR 302 from Anton Paar at different shear rates Figure 3.2b. The device provides high accuracy due to high precision air bearings and a powerful, synchronous motor drive. A rheometer is designed to work with different measurement geometries such as cone-plate, plate-plate, and cylindrical geometry Figure 3.2(a, c).

In this study, the concentric cylinder measuring system consisting of cup and bob (CC27) was used to measure the viscosity, and the measurements were performed under controlled shear rate. The measuring cup was filled with small volume (10 – 12) cm^3 of a homogenized solution, then the device was turned on. A software package provided with a rheometer gives full control over test settings such as temperature, range of shear rates, number of data points, and temporal interval for measurement. During viscosity measurements, four intervals of shear rates are pre-set at (0.01 – 1,000)s^{-1} to investigate the cyclic behaviour of the system. All viscosity measurements are conducted at 70 ± 0.1 °C.

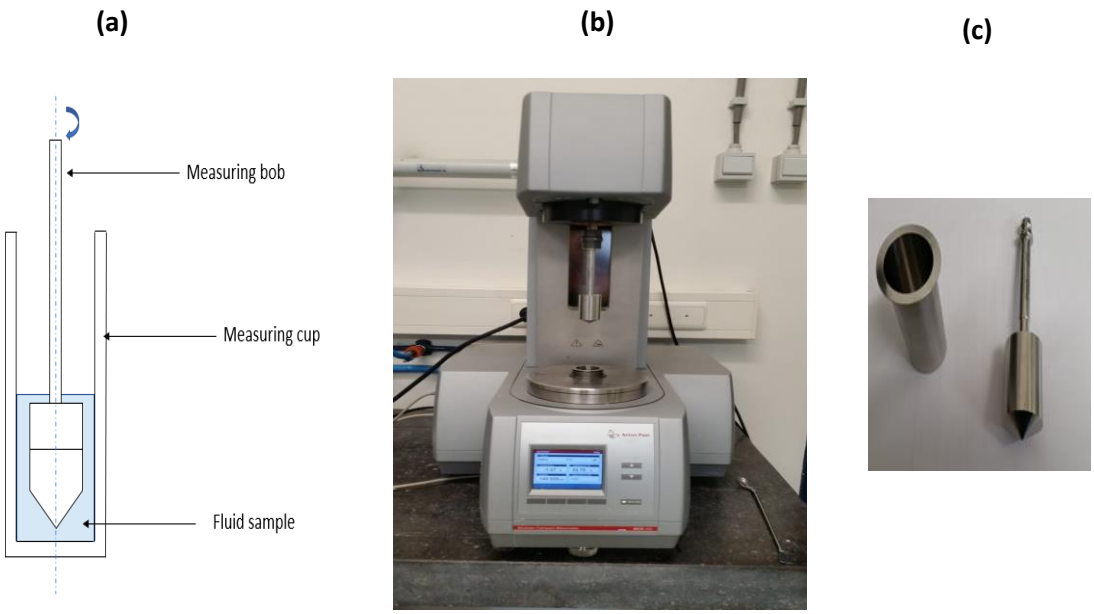

Figure 3.2. a) – Schematic of measuring system, b) – Photograph of rheometer device, c) – Measuring cup with bob

3.5.2 Core flood experiment

The sequence of procedures used to conduct the experiments is shown in Table 3.4 and Table 3.5. Each experiment started by ensuring all essential elements are in good condition and well connected. Then, setup is tested for any potential leakage using snoop and flushed with Carbon dioxide (CO_2) under pressure 5 ± 0.5 bar for 30 minutes to remove all the air from the system. The setup is vacuumed to remove any remaining gases, which might affect the compressibility of the system. Then, the dry core is saturated by injecting brine for enough pore volume, approximately 10 ± 0.5 PV to ensure pressure drop stabilization for each section and overall pressure drop along the core length as well. Saturation is done while maintaining a backup pressure of 25 ± 0.5 bar to dissolve any CO_2 and guarantee complete saturation of the sample with brine. The average permeability of the sandstone sample used in the experiment was found by varying the flow rate of injected brine and applying Darcy's law (Darcy 1856). For one phase experiments (i.e., Test1, Test2, Test3), adsorption and injectivity tests were conducted in steps presented in Table 3.4. Adsorption test is initiated through brine injection for 3PV at a low flow rate of 0.25 cm^3/min, which corresponds to the average fluid velocity in the reservoir. Then, chemical flooding is done at a flow rate of 0.25 cm^3/min, and the process ended again with brine injection, but for a larger pore volume. This is done to evaluate the amount of the chemicals adsorbed on the surface of the rock using effluents collected in plastic tubes. Injectivity test is conducted in the same steps, but for a higher flow rate to evaluate the injectivity loss due to chemical injection. In two-phase experiments (steps in Table 3.5), after core saturation, primary drainage is performed by injecting model oil for 2 PV, followed by bump flood for 1.5 PV to overcome end capillary effect, hence, to maximize the initial oil saturation. To obtain oil end relative permeability (k_{ro}), oil injection is varied to calculate (k_o). At this stage, irreducible water saturation (S_{wc}) is achieved. Subsequently, imbibition is conducted via brine injection (waterflood) and continued until no more oil is produced, which can be concluded when pressure drop over the core is constant. Experimental data; pressure drop, effluents are analyzed to calculate oil/ water cut, recovery factor, and cumulative oil production.

Table 3.4. The basic sequence of procedures used to conduct the single-phase experiments; Test 1: Polymer injection, Test 2: Nanofluid injection and Test 3: Polymer and Nanofluid injection

Steps	description		Flow rate (cm^3/min)	Backup pressure (Bar)	Injection direction
1	Leak test		-	-	-
2	CO_2 flushing		-	-	-
3	Core saturation		1	25	Up
4	Permeability test		(1,2,3,4 and 5)	25	-
5	Adsorption	Primary brine injection	0.25	25	Up
6	Adsorption	Chemical injection PAM/NP/(PAM-Np)	0.25	25	Up
7	Adsorption	Secondary brine injection	0.25	25	Up
8	Injectivity	Primary brine injection	2.5	25	Up
9	Injectivity	Chemical injection PAM/NP/(PAM-Np)	2.5	25	Up
10	Injectivity	Secondary brine injection	2.5	25	Up
11	Permeability test		(1,2,3,4 and 5)	25	Up

Table 3.5. The basic sequence of procedures used to conduct the 2phase experiments; Test 4: light oil (n-hexadecane), Test (5,6,7): Viscous oil (Ondina Shell oil).

Steps	description	Flow rate (cm^3/min)	Backup pressure (Bar)	Injection direction
1	Leak test	-	-	-
2	CO_2 flushing	-	-	-
3	Core saturation	1	25	Horizontal
4	Permeability test (k_{abs})	(1,2,3,4, and 5)	25	Horizontal
5	Oil injection	2	25	Horizontal
6	Bump flood	1.5	25	Horizontal
7	Permeability test (k_o)	(0.5,1,1.5)	25	
8	Water flooding	0.25	25	Horizontal
9	Bump flood	1.75	25	
10	Permeability test (k_w)	(0.25,0.75,1.25, 1.75)	25	
8	Polymer flooding	0.25	25	Horizontal

4

Results and discussion

During this study, several experiments are conducted using different medium including the bulk phase, porous media(sandstone) and microchips, details of microscopic experiments can be seen in Appendix F. In this chapter, the results relating to the viscosity modeling, single and two-phase core flood experiments are presented and discussed.

4.1 Polymer rheology

4.1.1 Polymer intrinsic viscosity

To determine the intrinsic viscosity for polymer solution at salinity 200,000 ± 1,000 mg/L and temperature 70 °C, the ratio of specific viscosity to concentration (reduced viscosity) is plotted against the polymer concentration. The experimental data (black markers) can be approximated using linear fitting equations. The intersection between both trend lines for low and high concentration indicates the critical overlap concentration, which represents the transition from dilute to semi dilute regime. The intrinsic viscosity is the limit of reduced viscosity as the solution concentration of polymer tends to zero (Sorbie 1991), and graphically it represents the Y-intercept of the first linear trend. The results are summarized in Table 4.1.

Table 4.1. Parameters obtained graphically from linear regression analysis of viscosity measurements at a zero-shear rate.

Salinity [S_s] (mg/L)	Temperature [T] (°C)	Intrinsic viscosity [η] (cm^3/gr)	Overlap concentration[C^*] (mg/L)
200,000 ± 1000	70 ± 0.1	880 ±20	5,870 ± 30

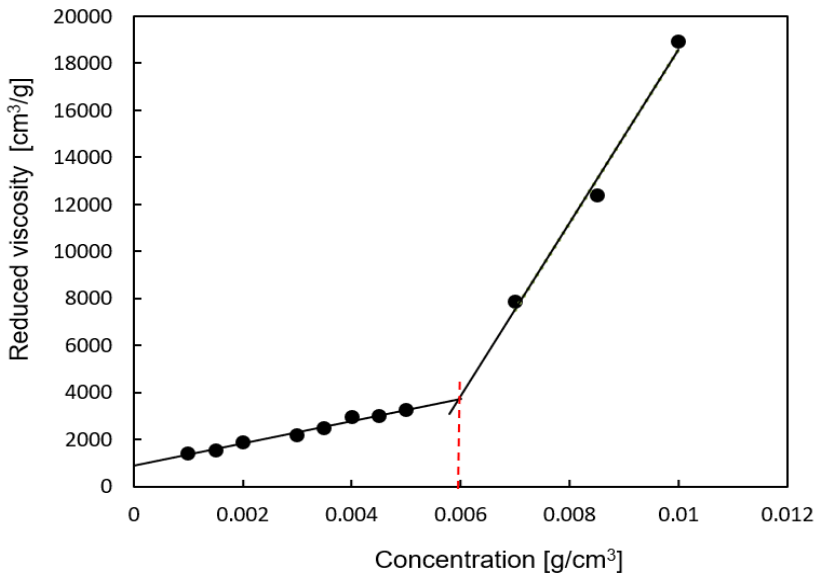

Figure 4.1. Rheological measurements (markers) fitted with linear equations for determining (C*) overlap concentration and [η] at 200,000 ± 1,000 mg/L salinity.

Figure 4.2 shows the results of polymer viscosity measurements conducted at atmospheric pressure, and temperature equals the required temperature for core flood experiments T=70 ±1℃. The viscosity of polymer PAM-98 with different concentrations dissolved in brine with high salinity (S= 200,000 ± 1,000 mg/L) is measured using MCR 302 rheometer from Anton Paar (see Table 4.2). These measurements are used to validate the Carreau-Yasuda model (see Eq.2.3) and to evaluate the behaviour of the polymer with a different shear rate, which can improve the design and execution during field treatment. The viscosity of brine is found to be around 0.65 ± 0.03 mPa.s, and the viscosity of the polymer is increased with increasing concentration. Figure 4.2 shows Newtonian behaviour for polymer at low concentration; the viscosity is almost constant with the shear rate because, at low concentration, the system is diluted; polymer molecules have more space to mobilize with the aqueous solution and intra-chain associations are dominant. Shear-thinning behaviour becomes more pronounced at higher concentrations and higher shear rates since applying high shearing weakens the intermolecular associations of long-chain hydrophobic groups. The symbols in Figure 4.1 indicate experimental data, while the continuous line represents the result obtained from the Carreau-Yasuda model.

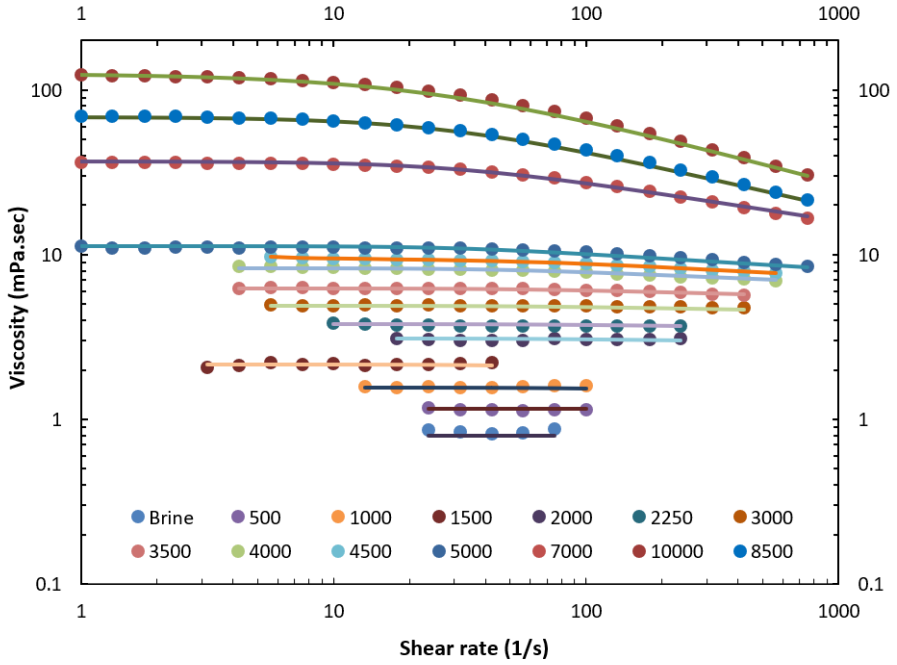

Figure 4.2. Experimental rheological measurements (symbols) modeled with the Carreau-Yasuda model (lines) at salinity 200,000 ± 1000 mg/L and temperature 70 ± 0.1 ℃.

Table 4.2. Parameters of the Carreau-Yasuda model (Eq.2.3) obtained from non-linear regression analysis of rheological measurements for polymer PAM_98 at different concentrations at T= 70 ± 0.1℃

Salinity (200,000 mg/L)					
C (mg/L)	n	a	η_0 (mPa.s)	η_∞ (mPa.s)	λ (s)
Brine	1.000	2	0.65	0.65	0.000
500	0.990	2	1	0.65	0.002
1000	0.990	2	1.57	0.65	0.010
1500	0.980	2	2.16	0.67	0.012
2000	0.970	2	3.10	0.65	0.014
2250	0.977	2	3.80	0.65	0.016
3000	0.970	2	4.90	0.65	0.017
3500	0.954	2	6.25	0.65	0.018
4000	0.928	2	8.30	0.65	0.022
4500	0.926	2	9.40	0.65	0.030
5000	0.900	2	11.30	0.65	0.032
7000	0.750	1.5	37.00	0.65	0.032
8500	0.637	1.3	69.00	0.65	0.036
10000	0.580	1	126.00	0.65	0.040

4.1.2 Effect of concentration (shear rate remains constant)

The viscosity of polymer solution at various concentration and constant salinity are measured. The results of shear viscosity are shown in (Table 4.2 and Figure 4.2). It can be observed that when some parameters, such as shear rate, salinity, and temperature are constant, then the viscosity increases with increase in the concentration of polymer solution. This can be because increasing the concentration, will increase the number of the molecules chain in the bulk volume which in turn increases the interactions with water molecules and leads to more resistance for fluid to flow. When the concentration increases further, the system reaches a semi diluted state, and the probability of chain interactions becomes larger. The chains get close to each other, and this will lead to more association between hydrophobic groups; a large coil and more inter-chain association, so viscosity is enhanced. However, at low concentrations, the possibility of interaction between chains is small due to the fact the polymer coils act independently and do not interact with each other since more space is available for polymer molecules to move around.

As concentration increases, the distance between coils decreases, hence coils association can occur, generating longer chains. When polymer molecules are subjected to shear forces, they will deform because of their flexibility. Thus, the polymer chains need a long time to relax and return to its original conformation. Therefore, the Newtonian plateau is less pronounced at higher concentrations. Data in (Table 4.2) validates this interpretation as it shows that relaxation time (it is the inverse of critical shear rate) increases with concentration.

4.1.3 Effect of shear rate (concentration remains constant)

To study the influence of shear rate on the behaviour of the polymer, the shear rate is varied in a wide range (1 – 1,000) s^{-1}. It can be seen from Figure 4.2 that at low concentration, below the critical association concentration, the polymer shows almost Newtonian behavior, where the viscosity did not change significantly with the applied shear rate. Because of low concentration, the system is still under the dilute regime and therefore, the associations between polymer chains still not developed.

At high concentration (above 5,000 mg/L), when the shear rate is augmented, the Newtonian behaviour is followed by shear-thinning behavior. This is due to the breakdown of the intermolecular hydrophobic association which yield to viscosity reduction. Polymer chains due to high shear rate are oriented in the same direction of fluid flow causing less flow resistance.

4.2 Single-phase flow characteristics using core flood experiments

4.2.1 Polymer injection

- Adsorption test

The objective of this test was to investigate the adsorption behaviour of polymer solution when it flows in a porous medium. It is well documented that adsorption will affect the absolute permeability of the rock and may cause a loss in polymer concentration. Quantity determination of polymer adsorption is crucial because the mass loss of polymer exerts a detrimental effect on sweep efficiency, oil recovery and will lead to high costs from an economic point of view. When the injection of first brine is ended, polymer slug is pumped, and the effluent of the experiment is directed to a fraction collector. The purpose of collected volume fractions is to measure the polymer and tracer concentration as a function of injected pore volume which helps to estimate the amount of polymer adsorption and the injected pore volume at which polymer breakthrough happens.

Brine with 200,000 ± 1,000 mg/L TDS is initially injected in the core to ensure complete saturation under backup pressure of 25.0 ± 0.5 bar, then the average permeability of the core is measured. The flow behaviour of PAM-98 is then examined through injecting 3 PV of primary brine followed by 7 PV injection of polymer solution into in the core at a constant volumetric rate of 0.250 ± 0.001 cm^3/min and concentration of 500 mg/L. The process of polymer injection is ceased after the predetermined amount of polymer is injected and the value of pressure drop (ΔP) over the core almost level off (reached steady state). Afterward 7.00 ± 0.05 PV of the same brine composition is injected and (*RF, RRF*) are evaluated. The pressure drop profile measured during the adsorption test can be seen in Figure 4.3

Experimental data used for retention quantification are differential pressure values across each section along with pressure drop over the entire core length. In addition, effluent samples collected at a specific time interval 40 min, were analysed with correlation to cumulative injected pore volume using TOC analyser and Spectrophotometer device, details can be found in Appendix (A and B).

Figure 4.3 shows the differential pressure over the entire core length. Polymer injection produces gradually higher pressure drops compared to brine and approximately after 1.5 ± 0.02 PV polymer breakthrough happens, then the trend tends to stabilize. When enough volume of polymer solution flows through a porous medium, steady-state is achieved; the pressure difference between the inlet and outlet of the core remains constant. Minor fluctuation in differential pressure profile is yet possible due to a long injection period, which requires running the experiment overnight, and this is necessary will yield to inevitable temperature fluctuation.

The increase in pressure drop is a consequence of energy loss or dissipation that can be due to interaction between the polymer molecules (viscosity) from one side, and friction between polymer solution and rock surface on the other side. Knowing that polymer at a temperature of 70 ± 0.1°C has viscosity 1 ± 0.03 mPa.s higher than brine 0.65 ± 0.03 mPa.s, already indicates a significant contributor in increasing the pressure drop.

Polymer adsorption on the rock surface will reduce the pore fraction available for polymer flow and cause additional pressure loss along with viscosity. In short, the pressure drops generated from

polymer injection can be due to higher polymer viscosity in comparison with brine Table 4.9 and its retention during transport in the porous medium.

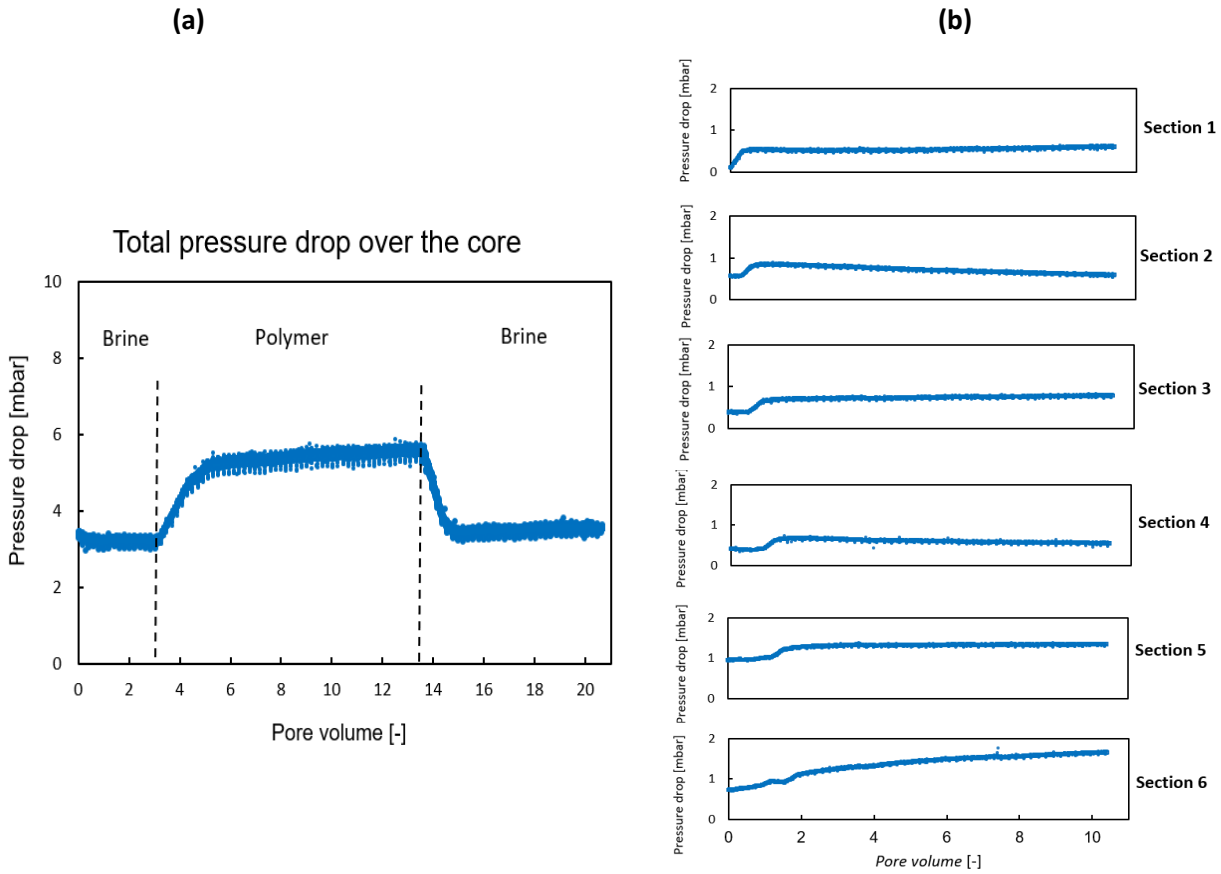

Figure 4.3, where a) – Differential pressure profile during polymer adsorption test (500) mg/L at a flow rate (0.25) cm^3/min, and b) – Differential pressure for each section.

Figure 4.3a also shows that total pressure drop is an integral of pressure drop on each section along with the core. At the beginning of each section in Figure 4.3b, a horizontal part with different time exists, which represents the pressure drop due to brine. This horizontal part is very short in section one because this section feels the polymer pressure directly after the polymer occupies the inlet lines and cap of the core holder. As polymer transports from one part to another, the total ΔP monotonically increases and persists till breakthrough occurs. However, the increasing rate may slightly be different from one section to another depending on the absolute permeability and amount of polymer adsorption inside every single section. Constant differential pressure over the core is only achievable if the pressure drop for each part of the sandstone core was stable, and this is only possible when rock adsorption is satisfied, and mass loss is controlled by tightening the pressure points on core holder. After injecting 10 ± 0.2 PV of polymer to ensure that the steady-state is reached, another 7 ± 0.05 PV of secondary brine is injected. Secondary brine injection into the core led to a higher pressure drop compared to primary brine. This can be attributed to permeability reduction due to polymer

adsorption. The sequence of the process is significant to investigate the adsorption behaviour of the polymer during the transport through the core. The polymer transport effects can be evaluated by calculating resistance factor *RF,* which represents mobility reduction, residual resistance factor *RRF,* which represents permeability reduction (adsorption-induced permeability effect), and estimating polymer retention. *RF and RRF* are calculated using pressure drop of brine and polymer at steady state using Eq.2.4 and Eq.2.5. The results are shown in Table 4.3 and Figure 4.4

Table 4.3. Resistance factor, which represents mobility reduction and residual resistance factor which represents permeability reduction during PAM-98 adsorption test.

Section	ΔP_b^0 (mbar)	ΔP_p (mbar)	ΔP_b^1 (mbar)	RF (-)	RRF (-)
1	0.58 ± 0.02	1.00 ± 0.03	0.71 ± 0.02	1.72 ± 0.07	1.22 ± 0.05
2	0.55 ± 0.02	0.85 ± 0.03	0.55 ± 0.02	1.55 ± 0.07	1.00 ±0.05
3	0.58 ± 0.02	0.91 ± 0.03	0.59 ± 0.02	1.57 ± 0.07	1.02 ± 0.05
4	0.59 ± 0.02	0.93 ± 0.03	0.55 ± 0.02	1.58 ± 0.07	1.00 ± 0.05
5	0.55 ± 0.02	0.84 ± 0.03	0.57 ± 0.02	1.53 ± 0.05	1.04 ± 0.05
6	0.59 ± 0.02	0.87 ± 0.03	0.60 ± 0.02	1.47 ± 0.07	1.02 ± 0.05
Over the core	3.23 ± 0.04	5.58 ± 0.04	3.54 ± 0.04	1.73 ± 0.02	1.10 ± 0.02

In addition, the measured steady-state pressure drops are converted into apparent viscosity using Darcy law,

$$\mu_{app} = \frac{q\ L}{k\ A\ \Delta P}$$

where k [m^2] is the absolute permeability, A [m^2] is the cross-sectional area, q [m^3/s] and ΔP [Pa] is the pressure drop along the core length, L [m]. By comparing the calculated apparent viscosity μ_{app} 1 ± 0.03 of polymer to the shear viscosity at an equivalent shear rate 6.5 ± 0.03 (see Table 4.9), it appeared that the polymer viscosity did not experience any change.

- Effluent analysis:

Samples collected during polymer slug injection at each 40 min interval with a constant injected flow rate of 0.25 cm^3/min were used for further analysis of the adsorption behaviour. Next, several samples were selected, and a small mass 1.50 ± 0.01 g of each sample was taken and diluted for total organic carbon measurement, the dilution factor of the effluent samples was 20 ± 0.05. Diluting the samples is important to ensure that the measuring TOC will be less than the maximum value 50 mg/L, which TOC analyser can handle and based on these measurements and polymer molar mass, polymer concentration is obtained. The steps of measuring TOC are explained in more detail in (Appendix B). On the other hand, to obtain a tracer profile, another small mass 0.070 ± 0.008 g was taken from each selected effluent and diluted 540 ± 20 times. Absorbance was measured at 226 nm wavelength using UV/Visible 4050 spectrophotometer, the details of tracer measurements can be seen in (Appendix A). The polymer and tracer profile are shown in Figure 4.4, and it is generally adopting S shape. Based on

the mass balance calculation, the polymer adsorption value was estimated 62.89 ± 7.70 µg/g rock (see Table 4.4).

The tracer effluent curve represents no adsorption case; base case, hence is usable as a reference. From Figure 4.4, it can be observed that 0.5 of normalized concentration of tracer corresponds to around 1.1 ± 0.1 PV, and by examining the normalized effluent curve of polymer, retardation of the polymer has been proven, and this indicates the presence of adsorption. Polymer breakthrough is estimated to be around 1.5 ± 0.2 PV.

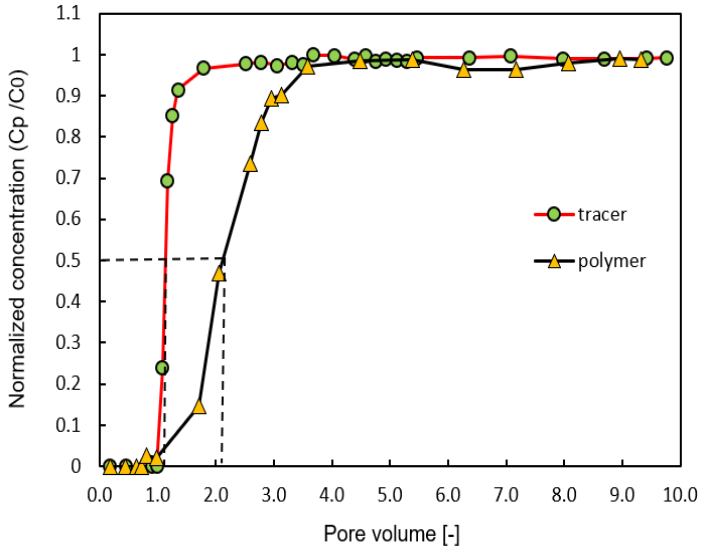

Figure 4.4. The effluent concentrations of Test 1, including both tracer and polymer versus cumulative pore volume.

After approximately 3.5 ± 0.2 PV, it is seen that the normalized concentration of polymer approaches to a reasonable extent the value of unity. It can be interpreted due to no mass transfer between adsorbed and flowing polymer, and a very small effect of filtration. No significant polymer filtration is observed at the inlet of the polymer.

Table 4.4. Parameters used to calculate the adsorbed amount of polymer

Δ(PV)@50% (-)	1.00 ± 0.03
Pore volume (cm^3)	108.00 ± 7.00
polymer C_0 (mg/L)	500 ± 30
Porosity (-)	0.25 ± 0.02
Bulk volume (cm^3)	432.08 ± 19.00
Grain density (g/ cm^3)	2.65 ± 0.05
Mass of sandstone grains(g)	858.76 ± 80.00
Adsorbed amount (µg/g rock)	62.89 ± 7.70

- Injectivity test

Adsorption test is followed by an injectivity test, that has a similar sequence of adsorption test. However, the injectivity test is conducted at a flow rate of 2.5 cm^3/min, which is higher than the flow rate in the adsorption test by factor 10. This flow rate corresponds to velocity which is 10 times higher than the average fluid speed in the formation, and it can be encountered as the fluid passes through perforations or flows near the wellbore region.

The purpose of the test is to ensure that the maximum pressure drop exerted of injecting chemical material at a concentration of 500 ± 30 mg/L and temperature 70 ± 1℃ are still below the fracturing pressure of the sandstone formation. The result of the test is shown in Figure 4.5

Similar to the adsorption test, injecting polymer after primary brine yields to higher pressure drop. This can be because polymer viscosity 1 ± 0.03 mPa.s is higher than brine viscosity 0.65 ± 0.03 mPa.s, so flow resistance will be higher. Another possible reason is that injecting polymer at a higher flow rate of 2.5 cm^3/min may lead to an additional retention mechanism associated with flow dynamics.

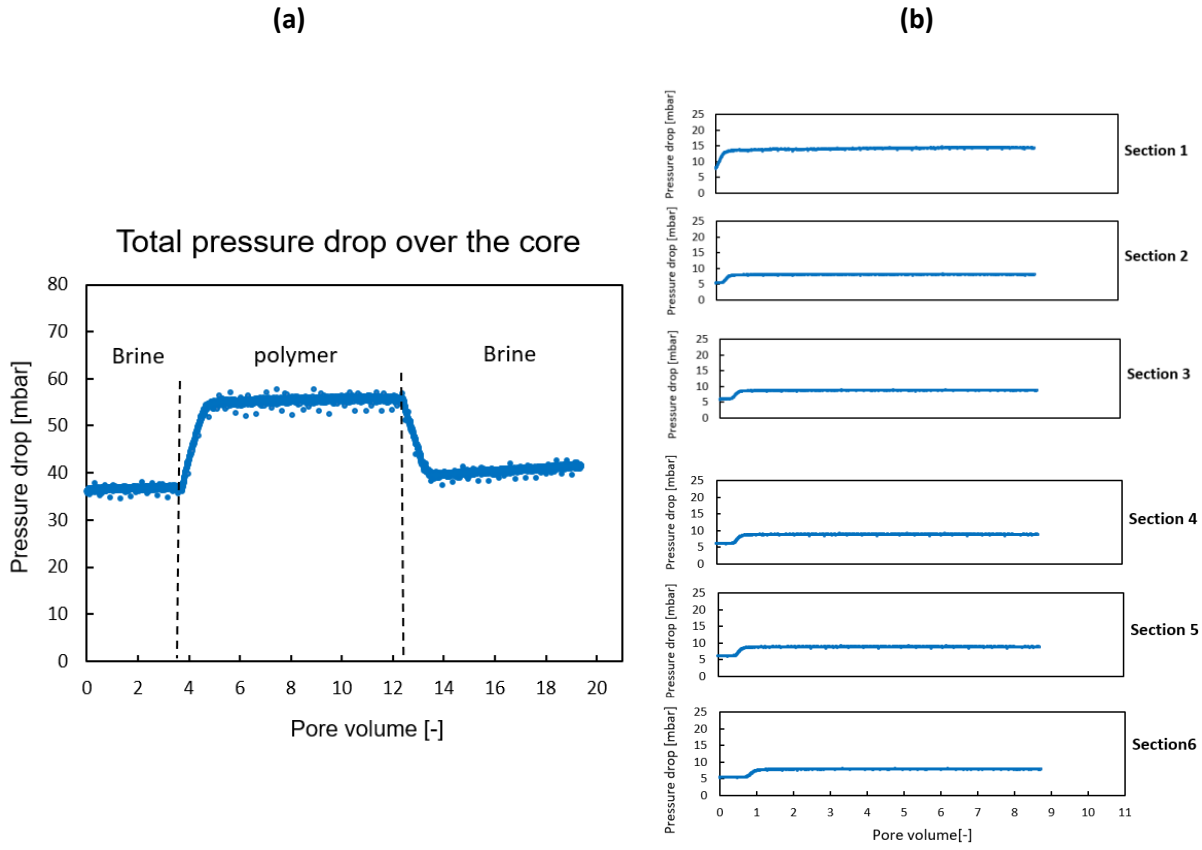

Figure 4.5, where a) – Differential pressure profile during polymer injectivity test (500) mg/L at flow rate (2.5) cm^3/min, and (b) – Differential pressure for each section.

Data presented in Table 4.3 and Table 4.5 shows that pressure drop increases with flow rate as should be expected. For instance, primary brine in adsorption test caused 3.23 ± 0.04 mbar over the core, while in injectivity test same brine caused 36.89 ± 0.04 mbar due to a higher injection flow rate.

Table 4.5. Resistance factor which represents mobility reduction, and residual resistance factor which represents permeability reduction during PAM-98 injectivity test.

Section	ΔP_b^0 (mbar)	ΔP_p (mbar)	ΔP_b^1 (mbar)	RF (-)	RRF (-)
1	8.34 ± 0.17	14.28 ± 0.31	12.98 ± 0.21	1.71 ± 0.05	1.56 ± 0.04
2	5.49 ± 0.10	8.00 ± 0.17	5.47 ± 0.08	1.46 ± 0.04	1.00 ± 0.02
3	5.98 ± 0.10	8.70 ± 0.19	5.95 ± 0.10	1.45 ± 0.04	1.00 ± 0.02
4	6.06 ± 0.13	8.77 ± 0.20	6.04 ± 0.10	1.45 ± 0.05	1.00 ± 0.03
5	5.50 ± 0.09	7.97 ± 0.18	5.51 ± 0.09	1.45 ± 0.04	1.00 ± 0.02
6	5.42 ± 0.11	7.81 ± 0.17	5.36 ± 0.08	1.44 ± 0.04	1.00 ± 0.02
Over the core	36.77 ± 1.10	55.49 ± 1.36	41.31 ± 0.69	1.51 ± 0.06	1.12 ± 0.04

4.2.2 Nanofluid injection

To evaluate the transport behaviour of Nanofluid dispersion (SNPs dispersed in brine with concentration 5,000 mg/L and TDS= 200,000 mg/ L), two tests were carried out. These tests are adsorption and injectivity test, and they were conducted in similar ways as it had been described in section 4.2.1.

- Adsorption test

The first slug of brine used in the adsorption test of SNPs, as can be seen in Table 4.6a, caused approximately the same pressure drops ΔP=3.5 mbar as in Test 1 and a very small difference in ΔP can be due to average rock permeability (see Table 3.2). As the SNPs fluid is injected into the core, the total pressure drop over the core gradually increases. At 4 PV, the differential pressure drops a little bit up to 5.5 PV. Afterward, the rate of pressure drop increases drastically and continues so till the end of SNPs injection. Then, secondary brine which has equal salinity as a primary slug is injected at the same flow rate of 0.25 cm^3/min. The differential pressure is increased at the start and then dropped at a high gradient.

To obtain a reasonable interpretation of this phenomenon, several available sources of data needed to be integrated. Therefore, a sample of nanofluid used for the adsorption test, and the inlet of the core is examined directly after the experiment. In addition, the pressure drop of each section is reviewed and compared with the other sections. Nanofluid samples showed a clear dispersed fluid, no trace of precipitation or agglomeration and no change in color. In addition, at the inlet of the sandstone core, a white layer of SNPs was observed. From Figure 4.6b, it can also be seen that the pressure drop increased significantly in section one; it indicates a filtration process at the inlet of the core which eventually forms a plug of SNPs. A small variation in pressure drop trend in each section may refer to instable adsorption within the core due to weak bond between pores and nanoparticles

or because of the measuring differential pressures of each section are within the error range of pressure gauges. *RF* and *RRF* are large, but they cannot be precisely calculated because the overall pressure profile did not reach a steady-state. Nevertheless, it was calculated based on the pressure drop values at the end of each process, see Table 4.6.

Table 4.6. The resistance factor represents mobility reduction and residual resistance factor which represents permeability reduction during the adsorption test of SNPs fluid.

ΔP_b^0 (mbar)	ΔP_{SNPs} (mbar)	ΔP_b^1 (mbar)	RF (-)	RRF (-)
3.5 ± 0.04	20.88 ± 0.04	7.41 ± 0.04	5.97 ± 0.01	2.12 ± 0.02

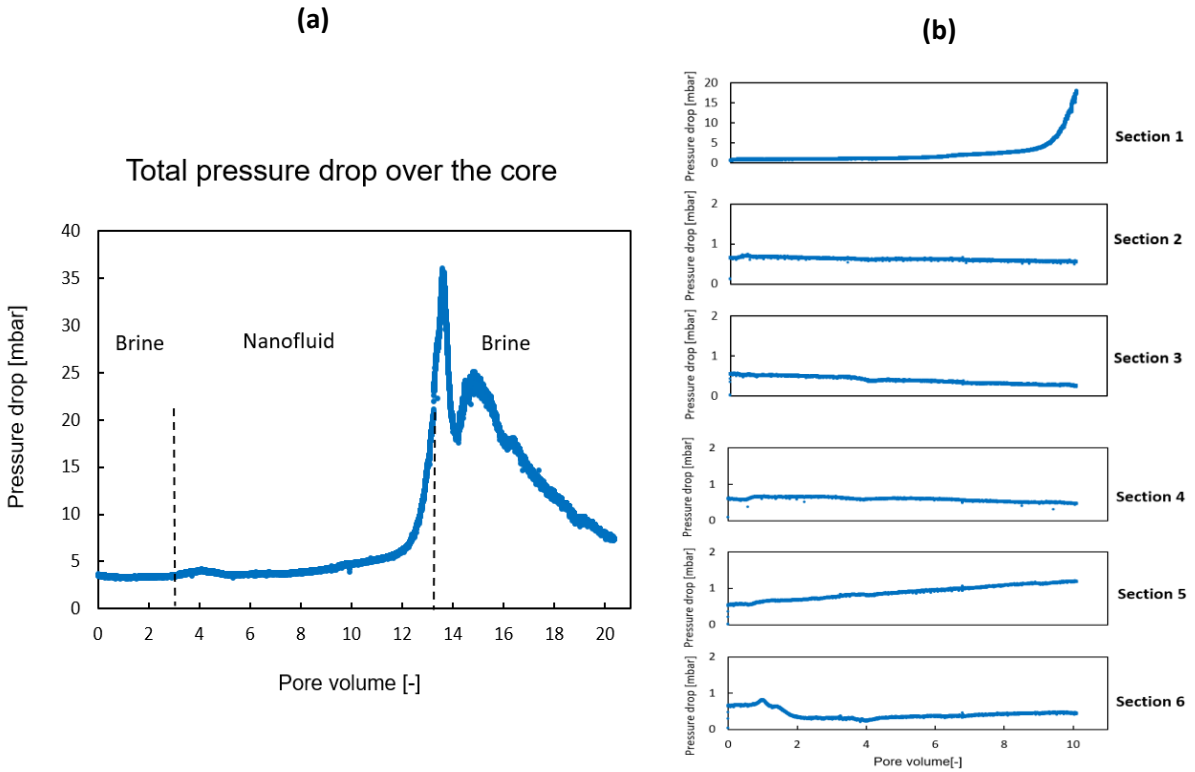

Figure 4.6, where a) – Differential pressure profile during nanofluid adsorption test (5,000) mg/L at a flow rate (0.25) cm^3/min, and b) – Differential pressure for each section.

- Effluent analysis

Experimental effluent during nanofluid injection is collected in each 40 min interval, and then several samples are selected for analysis to determine tracer and SiO_2 concentration. Tracer concentration is determined in the same method explained in section 4.2.1, while analysis for silica concentration is done using atomic absorption spectroscopy at the Analytische Laboratorien in Lindlar, Germany. The results are shown in Figure 4.7.

Normalized concentration curve for the tracer (KI) shows an expected result, i.e., normalized concentration is zero when the cumulative injected volume of nanofluid is less than 1 PV, and once it reaches this value, the normalized concentration increases very rapidly to reach the unity. This indicates that there is no physical and chemical interaction between tracer and sandstone (Sorbie 1991).

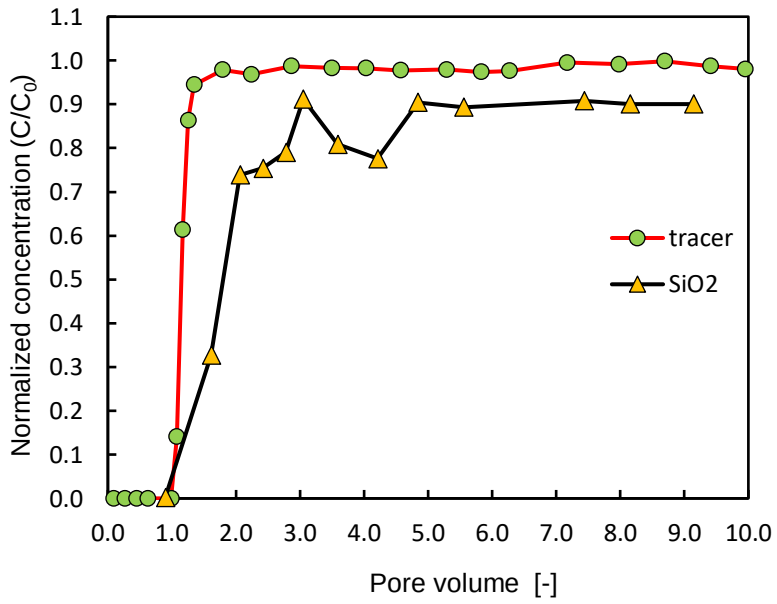

Figure 4.7. Effluent concentrations of Test 2, including both tracer and SiO_2 vs. cumulative pore volume

The normalized concentration curve for silica nanoparticles breakthrough happened at around 1.3 ± 0.2 PV. Between (2 – 5) PV, the slope of the silica curve fluctuates, which means that silica concentration at the outlet is not constant. This can be due to either silica adsorption is not stable or because of temporary blockage of some pores, which can contribute to fluid flow again when the pressure gradient becomes large enough to push the dispersion forward. After 7 PV, the curve of silica stabilizes and does not approach the unity because of particle agglomeration at the inlet of the core.

Table 4.7. Parameters used to calculate the adsorbed amount of nanoparticles

Δ(PV)@50% (-)	0.65 ± 0.03
Pore volume (cm^3)	108.00 ± 7.00
Nanoparticles C_0 (mg/L)	5,000 ± 70
Porosity (-)	0.25 ± 0.02
Bulk volume(cm^3)	432.10 ± 22.00
Grain density (g/ cm^3)	2.65 ± 0.05
Mass of sandstone grains(g)	858.76 ± 83.00
Adsorbed amount (µg SNPs/g rock)	408.81 ± 48.05

- Injectivity test

Figure 4.8 represents the results for the SNPs injectivity test. The pressure drop profile for all sections reached a steady state. Section one shows a higher pressure drop compared to other sections. This can be attributed to temperature effect and friction in extra elements such as inlet tubes and cap of core holder present before the fluid enters the core. The temperature of the injected fluid in inlet tubes may not reach the target due to the high injection rate of 2.5 cm^3/min. Thus, its viscosity will be slightly higher than the fluid in other parts. On the other hand, injected fluid passes through the transparent tube, metallic coiled tube, and core holder cap and that will cause additional pressure to drop.

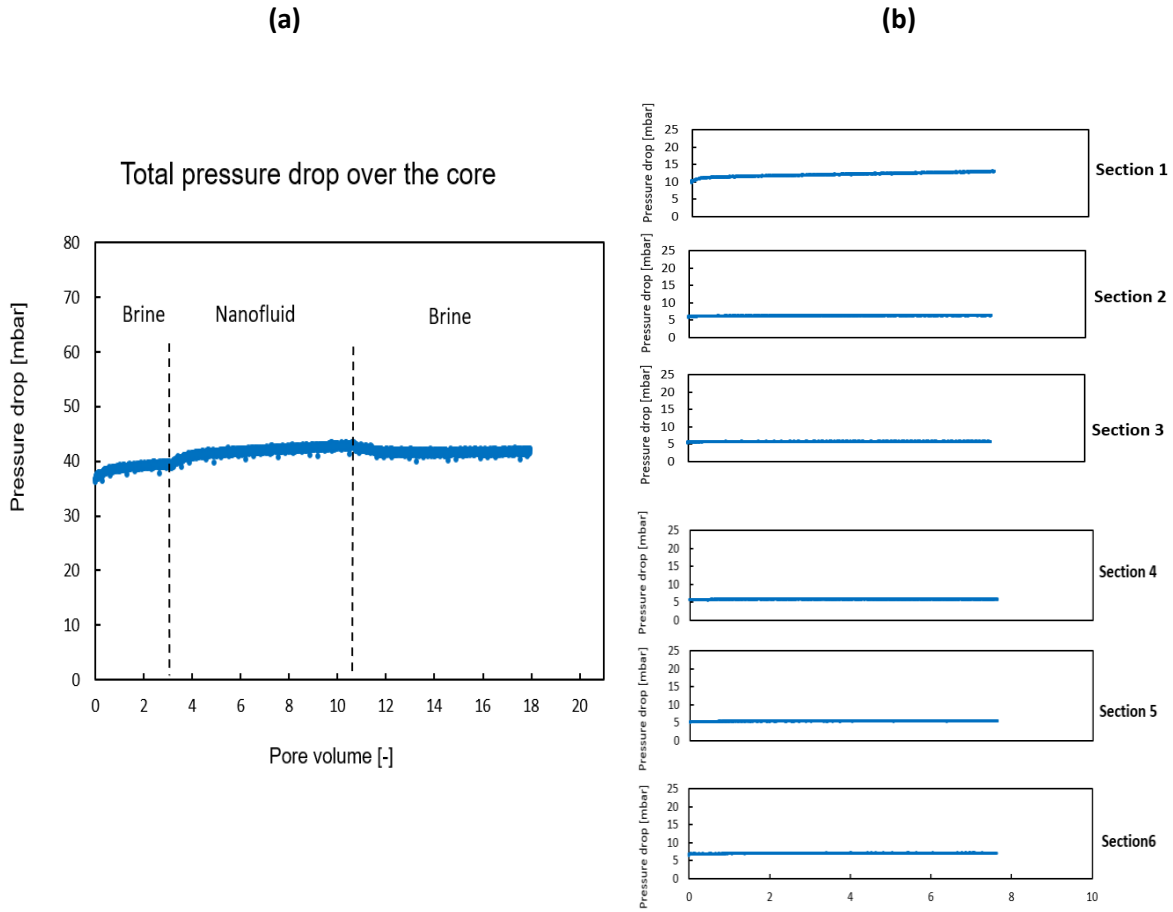

Figure 4.8, where a) – Differential pressure profile during nanofluid adsorption test (5,000) mg/L at a flow rate (2.5) cm^3/min, and b) – Differential pressure for each section.

Steady-state differential pressure produced from first brine, nanofluid and second brine injection for all sections are presented in Table 4.8. Data shows that pressure drop caused by nanofluid and second brine have almost the same values. This can be due to small viscosity difference between SNPs fluid and second brine where they have a viscosity of 0.75 ± 0.03 mPa.s and 0.65 ± 0.03 mPa.s respectively.

Table 4.8. The resistance factor represents mobility reduction and residual resistance factor which represents permeability reduction for all core sections during the injectivity test.

Section	ΔP_b^0 (mbar)	ΔP_{SNPs} (mbar)	ΔP_b^1 (mbar)	RF (-)	RRF (-)
1	10.4 ± 0.16	12.9 ± 0.18	12.7 ± 0.17	1.24 ± 0.03	1.22 ± 0.02
2	6.0 ± 0.08	6.2 ± 0.08	6.1 ± 0.07	1.04 ± 0.02	1.02 ± 0.02
3	5.5 ± 0.07	5.7 ± 0.08	5.6 ± 0.07	1.03 ± 0.02	1.00 ± 0.02
4	5.6 ± 0.09	5.8 ± 0.14	5.7 ± 0.10	1.02 ± 0.03	1.00 ± 0.02
5	5.2 ± 0.07	5.3 ± 0.06	5.2 ± 0.07	1.03 ± 0.02	1.00 ± 0.02
6	6.8 ± 0.09	6.9 ± 0.08	6.8 ± 0.08	1.03 ± 0.02	1.01 ± 0.02
Over the core	39.5 ± 0.63	42.7 ± 1.07	42.0 ± 0.69	1.08 ± 0.03	1.06 ± 0.02

4.2.3 Hybrid (polymer and nanoparticles)

The effect of introducing inorganic silica nanoparticles into hydrophobically modified polymer PAM-98 was investigated both in bulk by measuring the viscosity, and porous media through core flood. The bulk viscosity of the (PAM-98, SNPs) dispersion was measured at certain concentrations; 5,000 mg/L of SiO_2 and 500 mg/L of PAM-98, the temperature at 70 °C and brine salinity of 200,000 ± 1,000 mg/L. The results are presented in Figure 4.9 and Table 4.9. They show that the viscosifying power for a hybrid solution is enhanced in such harsh environments.

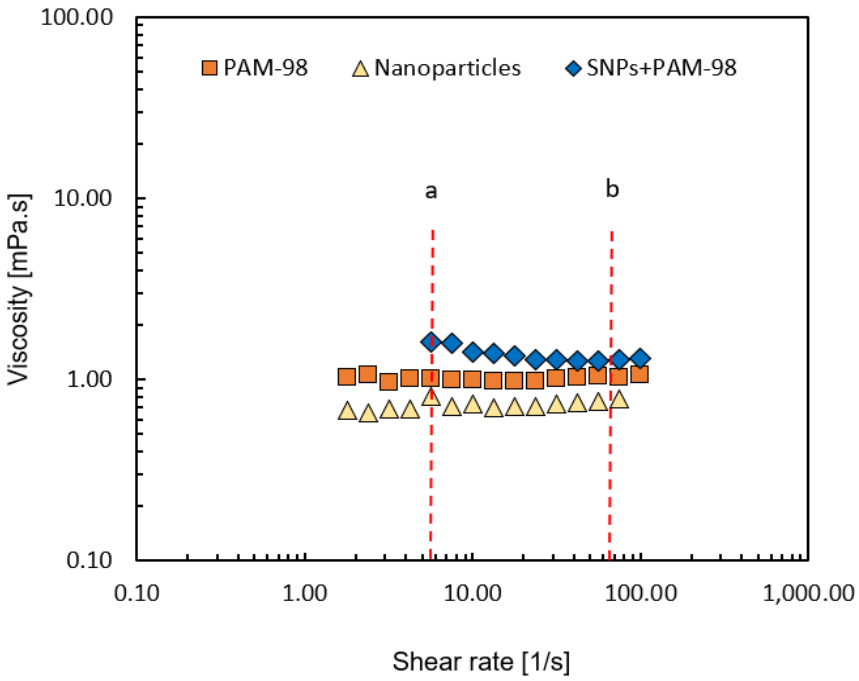

Figure 4.9. Viscosity measurement for PAM-98, silica nanoparticles and hybrid dispersion. (a) shear rate 6.5 1/s at 0.25 cm^3/min, and b) shear rate 65 1/s at 2.5 cm^3/min.

Fluids in the subsurface flow at an average velocity equal to 1ft /day, therefore equivalent shear rate 6.5 s^{-1} is calculated to determine the apparent viscosity in a porous medium using the exponent from the Carreau-Yasuda model (see Table 4.2) and rock properties such as porosity and permeability. The relation of equivalent shear rate was given by (Cannella, 1988)

$$\gamma_{eq} = C \left(\frac{3n+1}{4n}\right)^{\left(\frac{n}{n-1}\right)} . \left(\frac{u}{\sqrt{k.\varphi}}\right) \qquad \text{Eq.4.1}$$

γ_{eq}: equivalent shear rate in the porous medium, n: exponent from Carreau-Yasuda model, u: Darcy velocity, C: a constant accounting for porous media structure and k, φ: permeability and porosity of sandstone, respectively. The calculated equivalent shear rate is 6.54 ± 0.5 s^{-1}, and the corresponding apparent viscosity was summarized in Table 4.9.

Table 4.9. Comparison between viscosities of PAM-98, silica nanoparticles and PAM-98/ SiO_2 dispersion at T=70 ℃, salinity TDS =20%

Chemical Material	PAM-98	SNPs	PAM-98+SNPs
μ (mPa.s) at 0.25 cm^3/min	1.00 ± 0.03	0.75 ± 0.03	1.41 ± 0.03
μ(mPa.s) at 2.5 cm^3/min	1.00 ± 0.02	0.75 ± 0.03	1.26± 0.03

- Adsorption test

From Figure 4.10a, it can be seen that injecting hybrid dispersion exhibits different behaviour than injecting only SNPs fluid. Primary brine of 3.0 ± 0.1 PV was injected and it was enough to reach steady-state, followed by 1 ± 0.1 PV of Hybrid dispersion injected at q=0.25 cm^3/min. Dispersion breakthrough occurred around 1.8 ± 0.1 PV, and differential pressure over the core reaches a steady state after 3 ± 0.1 PV, without any indication of plugging or agglomeration as it was seen during nanofluid test, see Figure 4.7. Thus, it can be concluded that the presence of the polymer with nano-silica forms a new molecular conformation which improved the transport behaviour and stability for nanofluids. After Hybrid dispersion, 7.0 ± 0.1 PV of secondary brine was injected. The differential pressure will only start to drop after secondary brine fills the inlet tubes and enter the core. As can be seen from Figure 4.10b, almost all the sections have stable differential pressure except section 5. This can be due to either small leaks in ΔP points or malfunction in a pressure transmitter.

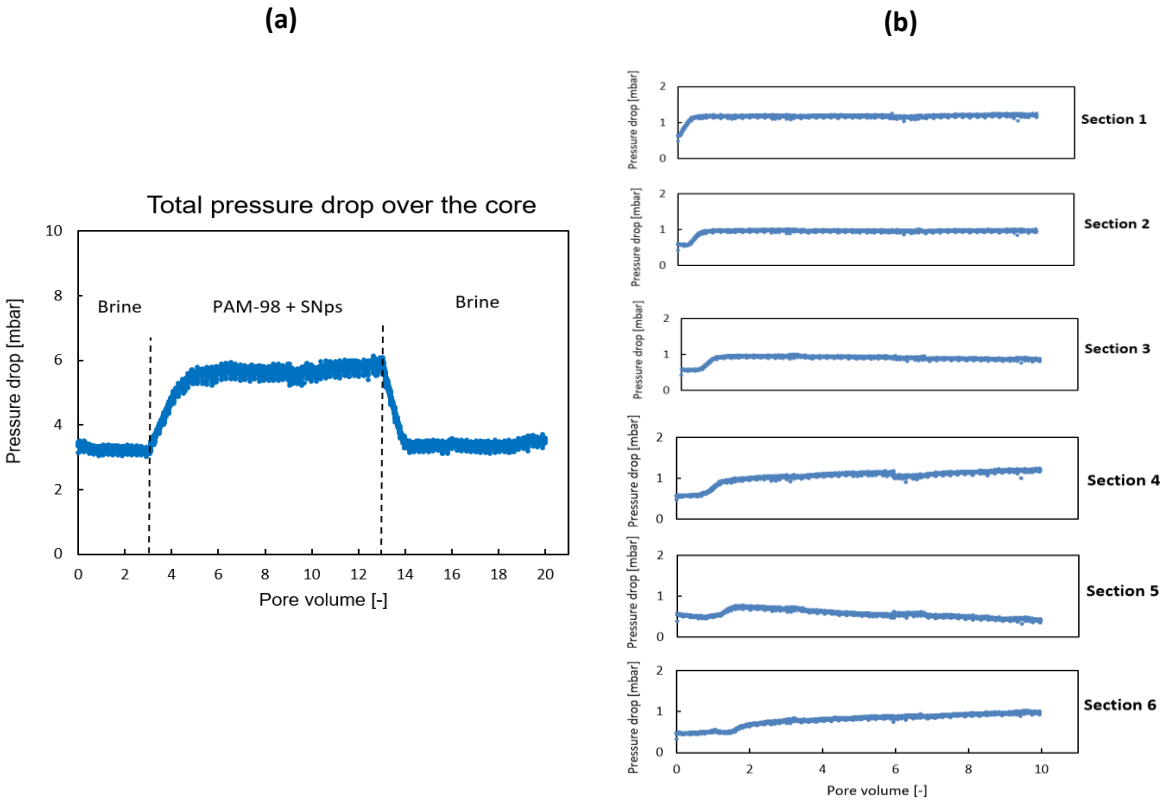

Figure 4.10, where a) – Differential pressure profile during adsorption test of SNPs dispersion with concentration of 5,000 mg/L SNPs and 500 mg/L PAM-98, the flow rate at 0.25 cm³/min, b) – Differential pressure for each section.

The measured steady-state pressure drop ΔP = 5.88 ± 0.26 mbar are converted into apparent viscosity using Darcy law. By comparing the calculated apparent viscosity, μ_{app} 0.95 ± 0.03 mPa.s of hybrid dispersion to the shear viscosity at the equivalent shear rate (see Table 4.9), it appeared that hybrid dispersion has lower apparent viscosity, which could be due to silica retention at the first section.

Table 4.10. Resistance factor, which represents mobility reduction and residual resistance factor which represents permeability reduction for all core sections during adsorption test.

Section	ΔP_b^0 (mbar)	ΔP_{HS} (mbar)	ΔP_b^1 (mbar)	RF (-)	RRF (-)
1	0.61 ± 0.02	1.11 ± 0.11	0.96 ± 0.02	1.81 ± 0.1	1.57 ± 0.04
2	0.56 ± 0.02	0.96 ± 0.05	0.50 ± 0.01	1.72 ± 0.06	0.90 ± 0.05
3	0.53 ± 0.02	0.96 ± 0.06	0.40 ± 0.02	1.79 ± 0.07	0.75 ± 0.06
4	0.65 ± 0.03	0.90 ± 0.19	0.77 ± 0.04	1.39 ± 0.22	1.19 ± 0.06
5	0.60 ± 0.04	0.91 ± 0.26	0.21 ± 0.01	1.51 ± 0.38	0.36 ± 0.20
6	0.73 ± 0.02	0.98 ± 0.04	0.39 ± 0.01	1.33 ± 0.05	0.53 ± 0.05
Over the core	3.23 ± 0.03	5.88 ± 0.26	3.54 ± 0.08	1.82 ± 0.05	1.10 ± 0.02

- ## Effluent analysis

Effluent samples were collected at the outlet of the core at 40 min time intervals. They were then analyzed for tracer, SNPs and polymer concentration, and the results are shown in Figure 4.11. Normalized concentration for tracer was calculated in the same method as previous tests (1, 2), while PAM-98 and SiO_2 concentration was calculated based on the Si concentration and TOC analysis of the effluents according to the next steps:

- S_i : The concentration that has measured is converted to SiO_2 by the following relation:

$$C_{SiO_2} = C_{S_i} \left(\frac{M_{SiO_2}}{M_{Si}}\right)$$

M_{SiO_2}, M_{Si}: molar mass of the Silica nanoparticles and Silicon, respectively.

- Total organic carbon of 1 mg/L of SiO_2 was measured to be 0.072 mg/L and based on that TOC of SiO_2 was calculated.

- $\text{TOC polymer} = \text{TOC (SiO2 + polymer)} - \text{TOC}(SiO_2)$

- $C_{PAM-98} = TOC_{polymer} \left(\frac{M_{carbon\ in\ polymer}}{M_{carbon}}\right)$
  C_{PAM-98} is the concentration of the polymer (mg/L), $TOC_{polymer}$ is the total organic carbon of the polymer (mg/L).

- Normalized concentration of polymer = concentration of polymer at each sample/ original concentration of polymer

The tracer passes through 0.50 ± 0.03 normalized concentration at 1.00 ± 0.02 PV, whereas, the retardation in the polymer and SNPs profile indicates the presence of adsorption in the core. Irregular behaviour of silica can be observed in Figure 4.11, and at 6.0 ± 0.2 PV, there is an increase in silica concentration above the unity. This can be due to the local accumulation of particles, which is released by a continuous injection process.

To obtain the adsorbed amount of polymer and SNPs on the rock surface, the mass of the rock grains was calculated considering the density of grains equal to 2.65 ± 0.03 g/l. The following equations were used for the calculation:

$$m_s = V_b . \rho_s (1 - \varphi) \qquad \text{Eq.4.2}$$

m_s: the mass of rock grains (g), V_b is the bulk volume (cm^3), ρ_s is the density of sandstone grains (g/l), and φ is bulk porosity.

$$M = \Delta(PV).PV . \frac{C_0}{1000} . \frac{1}{m_s} \qquad \text{Eq.4.3}$$

where M is the adsorbed amount of injected chemical (mg/g rock), $\Delta(PV)$ is the difference in injected pore volume between 50% normalized concentration of tracer and chemical material. PV is rock pore volume (cm^3) and C_0 is the initial concentration of the chemical material (mg/L). The results of the adsorption amount of polymer and nanoparticles are summarized in Table 4.11.

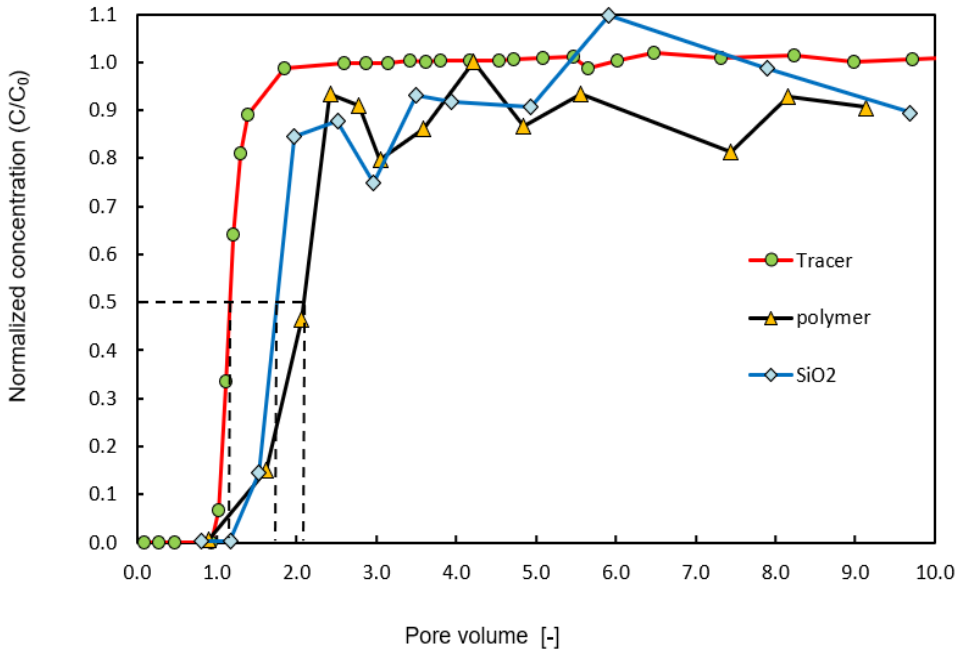

Figure 4.11. Effluent concentration vs cumulative pore volume, (PAM+ SNPs) with concentration 500 mg/L

Table 4.11. Parameters used to calculate the adsorbed amount of nanoparticles

Δ(PV)(polymer-tracer) @50% (-)	0.95 ± 0.1
Δ(PV)(SNPs-tracer) @50% (-)	0.60 ± 0.10
Pore volume (cm^3)	108.02 ± 6.00
Polymer C_0 (mg/L)	500 ± 30
Nanoparticles C_0 (mg/L)	5,000 ± 500
Porosity (-)	0.25 ± 0.02
Bulk volume (cm^3)	432.08 ± 17.28
Grain density(g/cm^3)	2.65 ± 0.05
Mass of sandstone grains(g)	858.76 ± 1.88
Adsorption amount of polymer (µ g PAM/g rock)	59.75 ± 7.10
Adsorption amount of SNPs (µ g /g rock)	377.36 ± 56.35

- Injectivity test

Figure 4.12 represents the results of the injectivity test for Hybrid dispersion (PAM-98 and SNPs). In Figure 4.12a, the primary brine of viscosity 0.65 ± 0.03 mPa.s was injected at a flow rate of 2.5 cm^3/min for 3.00 ± 0.1 PV and the value of pressure drop at the end of injected pore volume was 36.65 ± 1.00 mbar. The process was followed by injecting the hybrid dispersion with viscosity 1.41 ± 0.03 mPa.s It can be observed that once the hybrid dispersion was injected, the pressure drop increased gradually till breakthrough happened after 1.20 ± 0.02 PV. Then the differential pressure over the core reached steady state 60.00 ± 0.5 mbar after injecting 10.00 ± 0.10 PV. Finally, secondary brine was pumped for 7.00 ± 0.10 PV, and the value of pressure drop was 38.97 ± 0.5 mbar.

Figure 4.12b shows that the pressure drop for all sections was reached a steady-state, and the value of pressure drop was 8.50 ± 0.30 mbar except for section one, which had a higher pressure drop 15± 0.30 mbar. The reason is explained in the previous adsorption test, which is due to the additional pressure drop in inlet tubes and cap of core holder.

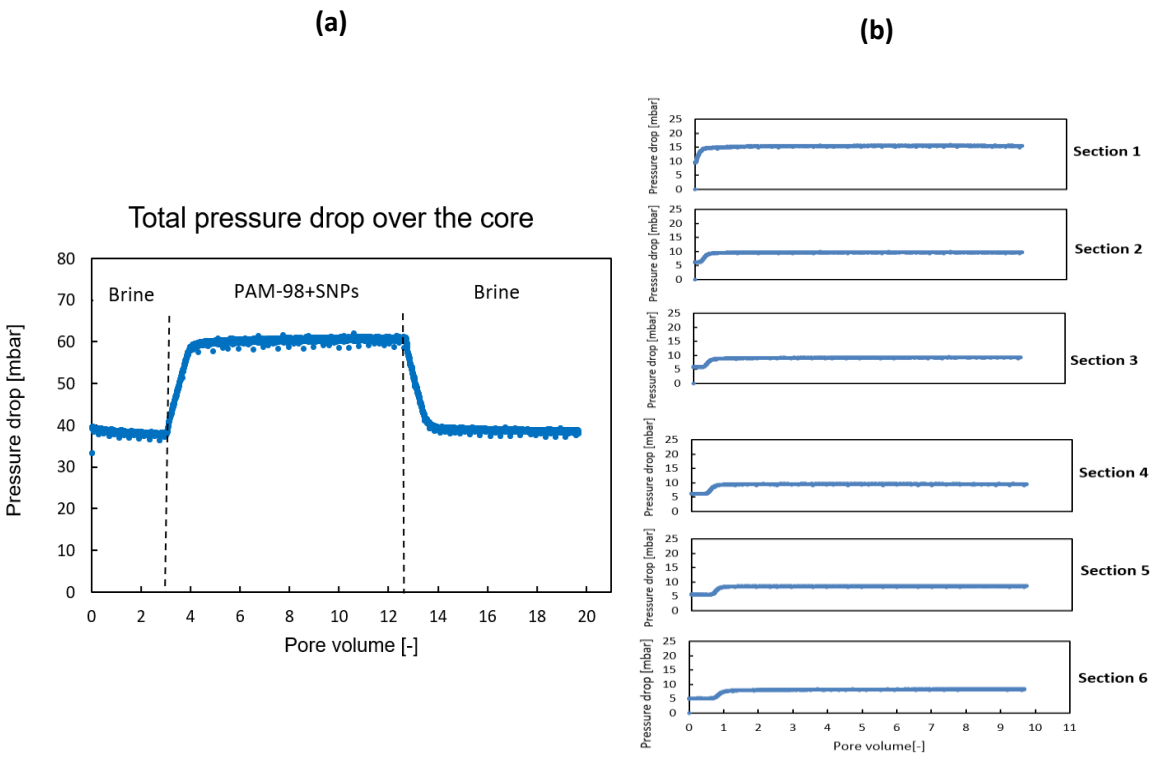

Figure 4.12, where a) – Differential pressure profile during the injectivity test of SNPs dispersion with concentration of 5,000 mg/L SNPs and 500 mg/L PAM-98, the flow rate at 2.5 cm3/min, b) – Differential pressure for each section.

Figure 4.12 outlines the results of differential pressure generated from injecting various chemical material during the injectivity test. The pressure drop value during injectivity is higher than these in adsorption tests approximately by factor 10, due to the fact that flow rate in adsorption test is 10 times less than the flow rate in the injectivity test. On the other hand, the pressure drop produced from injecting primary and secondary brine is less than the hybrid solution, and that can be attributed to the viscosity difference (see Table 4.9). Further, it can be seen that injecting secondary brine either

in adsorption or injectivity test causes pressure drop higher than primary brine. That can be interpreted by the impact of hybrid dispersion on the permeability of the core since amount of SNPs and polymer can be retained in the core, and that was found and quantified in the effluent analysis section.

Table 4.12. The resistance factor represents mobility reduction and residual resistance factor which represents permeability reduction for injectivity tests of hybrid combination.

Section	ΔP_b^0 (mbar)	ΔP_{HS} (mbar)	ΔP_b^1 (mbar)	RF (-)	RRF (-)
1	8.97 ± 0.22	15.46 ± 0.43	9.58 ± 0.15	1.72± 0.04	1.07±0.03
2	6.23 ± 0.16	9.63 ± 0.26	6.22 ± 0.10	1.55± 0.04	1.00±0.03
3	5.82 ± 0.15	9.24 ± 0.26	5.93 ± 0.09	1.59± 0.04	1.02±0.03
4	6.19 ± 0.18	9.46 ± 0.33	6.19 ± 0.09	1.53± 0.05	1.00±0.03
5	5.80 ± 0.14	8.51 ± 0.23	5.48 ± 0.09	1.47± 0.04	0.94±0.03
6	4.91 ± 0.12	8.17 ± 0.21	5.41 ± 0.07	1.66± 0.04	1.10±0.03
Over the core	37.93± 0.92	60.40 ± 1.59	38.82 ± 0.64	1.59± 0.04	1.02±0.03

4.3 Two-phase core flood experiments result

4.3.1 Viscous oil (Ondina shell oil4) displacement using high salinity brine (secondary recovery) and Hybrid solution (tertiary recovery)

In this experiment, the core from the previous test (Ondina3, results are shown in Appendix C) was reused. The core was utilized after the Quzix pump was checked and calibrated to avoid any pressure fluctuations related to the poor performance of the water pump, and thus to obtain more reliable outcomes during water flooding. Table 4.13 summarizes the main results of the experiment, which consists of different processes such as primary drainage, forced imbibition, followed by a combination (PAM-98+SiO2) injection.

Table 4.13. Summary of two-phase core flood experiment where PAM+SNPs used as tertiary recovery

Process	Parameters	
Oil Saturation	Oil breakthrough at pore volume (-)	0.31 ± 0.02
	Total water produced, Wp (cm^3)	54.00 ± 2.00
	Dead volume (cm^3)	17.95± 2.00
	Oil initially in place, OIIP (cm3)	36.05± 2.80
	Oil left over (previous test) (cm^3)	48.75± 2.00
	Initial oil saturation, S_{oi} (%)	78.52± 0.04
	Connate water saturation, S_{wc} (%)	21.48± 0.04
	Oil effective permeability, k_o (mD)	1532.65± 170.00
	Oil relative permeability, k_{ro}(-)	0.52± 0.07
	Oil viscosity at 70 ℃, μ_o (mPa.s)	15.95± 0.10
	Oil mobility, λ_o	0.03± 0.01
Waterflood	water breakthrough at pore volume (-)	0.34 ± 0.02
	Total oil produced, Wp (cm^3)	57.33 ± 3.00
	Dead volume(cm^3)	17.94 ± 2.00
	Residual oil saturation, S_{or_wF}(%)	42.05 ± 0.08
	Recovery factor, R_{f_wf} (%)	46.45± 5.00
	Water effective permeability, k_w(mD)	307.44 ± 30
	Water relative permeability, k_{rw} (-)	0.10 ± 0.02
	water viscosity at 70 ℃, μ_w (mPa.s)	0.65 ± 0.03
	water mobility, λ_w	0.15 ± 0.03
	Mobility ration $M_{w/o}$	4.72 ± 1.80
Polymer + SNPs	Polymer breakthrough at *PV* (-)	1.5 ± 0.02
	Total oil produced, Wp (cm^3)	0.00
	Dispersion effective permeability, k_H(mD)	490.96 ± 54.00
	Dispersion relative permeability, k_{rH} (-)	0.16± 0.02
	Dispersion viscosity at 70 ℃, μ_H (mPa.s)	1.41± 0.03
	Dispersion mobility, λ_H	0.11 ± 0.01
	Mobility ration $M_{(HS/w)}$	0.73± 0.1

From Table 4.13, it can be observed that oil breakthrough occurred at low pore volume 0.31 ± 0.02 due to the fact that a considerable amount of oil 48.75 ± 2 cm^3 was left in the core before using it in this test, due to a poor capacity of water to flush the viscous oil from sandstone because of capillary forces and low mobility ratio.

Figure 4.13 shows the total pressure drop recorded over the core during oleic phase injection at flow rate 0.5 cm^3/min along with oil and water cuts associated with primary drainage. Once the oil reaches the core inlet, pressure drop increases quickly with high slope due to capillary entry pressure and continues building up until oil breakthrough happens at approximately 0.31 ± 0.02 PV. Then, Pressure drop decreases gradually and eventually reaches an average steady-state of 315.00 ± 2.00 mbar at 2.00 ± 0.02 PV corresponding to oil flow at S_{wc}. Early breakthrough, as explained previously, happened because the amount of oil 48.75 ± 2.00 cm^3 was left from the previous test inside the core and was difficult to extract owing to capillary effect at pore scale and oil snapping off.

It can also be observed that water cut is equal to the unity until oil breakthrough takes place. After the breakthrough, oil cut increases immediately, and only a small amount of water will be produced. This can be attributed to the high viscosity of the oil, which can sweep a large amount of water, but after oil breakthrough, two-phase flow starts, and little amount of water will be drained with oil. It is worth mentioning that changing flow rate can create new dynamic forces which can either increase or decrease the amount of produced water after breakthrough.

Oil bump flood was conducted at higher injection rate 1.5 cm^3/min, to maximize the core saturation by overcoming the capillary end effect, and it reached an average steady-state of 842 ± 3 mbar at 1.5 ± 0.02 PV. After that, the injection flow rate was varied (0.5, 1, 1.5) cm^3/min to obtain oil relative permeabilityk_{ro}

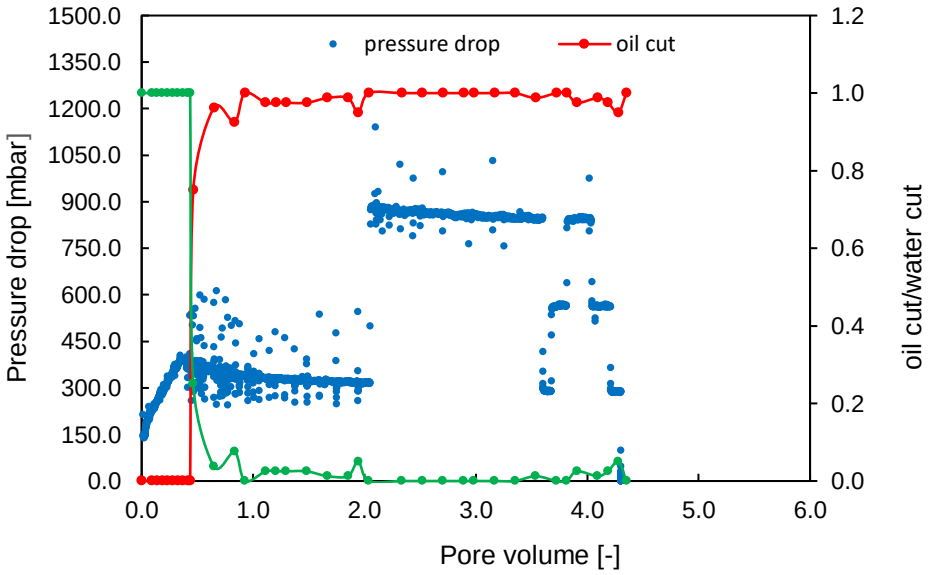

Figure 4.13. Total pressure drop profile during oil saturation(drainage), Ondina4

Forced imbibition process (see Figure 4.14) is conducted by injecting water at a flow rate of 0.25 cm^3/L for 5 ± 0.02 PV. During waterflooding, lower pressure drops were obtained with an average value of 36.5 ± 2 mbar due to lower flow rates and low viscosity of brine 0.65 ± 0.03 mPa.s in comparison to oil viscosity 15.95 ± 0.10 mPa.s. Water breakthrough happened at 0.34 ± 0.02 PV, after that, small spikes and fluctuations can be observed because of two-phase flow and sensitivity of backup pressure to viscosity difference between water and oil as they pass through. Similar to the drainage process, bump flood was done at 1.75 cm^3/min to maximize the ultimate oil recovery ($R_{f_{wf}}$) and achieve more realistic S_{or_wF}.

In addition to the pressure drop profile of water flooding, Figure 4.14 also shows a profile of differential pressure across the core as a result of injecting the dispersion, which represents a combination of PAM-98 and SNPs. The dispersion is injected at a flow rate of 0.25 cm^3/min for 3.00 ±0.02 PV. Breakthrough happens at around 1.50 ±0.02 PV since a small amount of polymer and SNPs get adsorbed on the rock surface. Although dispersion was injected at the same flow rate as water, it caused higher pressure drops 46 ± 1 mbar comparing to water due to permeability reduction because of adsorption and higher viscosity of dispersion 1.41 ±0.03 mPa.s.

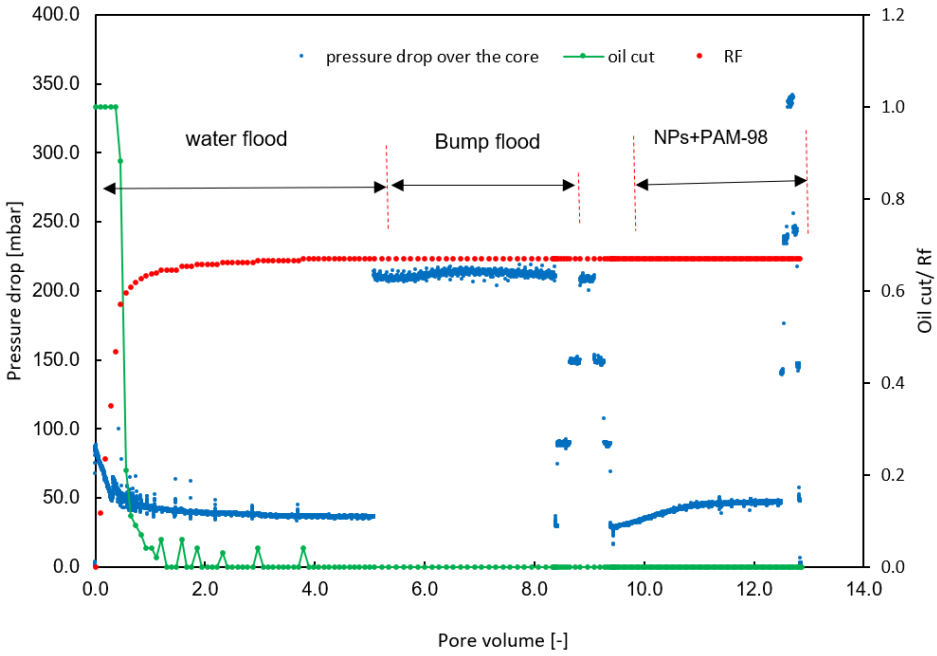

Figure 4.14. Total pressure drop profile during water flooding (forced imbibition), Ondina4

Table 4.13 shows cumulative oil production due to water flooding. At the beginning of the process, water flooding sweeps a large amount of oil effectively, and this is manifested in cumulative oil production where it increases linearly at high slope due to relatively good permeability of the core 3037.25 ± 350 mD. Before water breakthrough, only oil is produced at the outlet, and the amount of production is equal to the amount of water injected in the system. Early breakthrough happens at 0.34 ± 0.02 PV owing to unstable viscous fingering, where fingers of displacing fluid develop at the oil-water interface, forming inefficient contact zone due to viscosity contrast between water and

displaced oil (see Table 4.13). Therefore, two-phase flow starts, and the slope of the curve decreases rapidly because very small oil is produced. Eventually, no more oil will be produced until the end of the water injection, including bump flood and permeability test, and that is why the curve becomes a horizontal line. The dispersion (PAM-98, SNPs) is tested to appraise their viability for improving the final oil recovery, but unfortunately, no oil was produced.

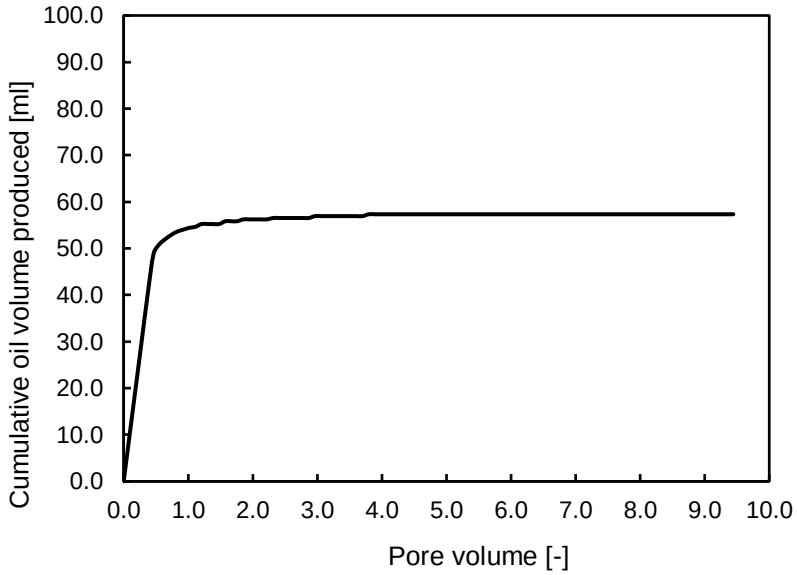

Figure 4.15. Cumulative viscous oil production produced by water, where dispersion did not produce any additional oil, therefore the plot is limited to waterflood only

5

Conclusion and recommendation

This chapter outlines the main conclusions that can be drawn based on this work and also suggests further recommendations for future research.

- Hydrophobically modified polymer was tested at different shear rates (1 – 1,000) s^{-1} and at high temperature 70 ± 1 ℃ and salinity 200,000 ± 1,000 mg/L, exhibited shear thinning behaviour at the relatively high range of concentration, and this behaviour was less pronounced or absent in low concentration.

- Introducing silica nanoparticles into hydrophobically modified polymer results in viscosity enhancement approximately 40 %, at the temperature 70 ± 0.1 ℃ and shear rate of 6.5 ± 1.0 s^{-1}, which can lead to better mobility control.

- Adsorption test using only polymer solution with concentration 500 mg/L indicated mobility reduction around 0.73 ± 0.02 since polymer has a higher viscosity than the brine which is used to saturate the core, and permeability reduction of 0.10 ± 0.02 due to polymer retention. The amount of polymer retained in the porous media was estimated to be around 62.89 ± 7.80 µg/g rock based on the effluent analysis.

- Silica nanofluids at concentration 5,000 mg/L appeared to clog the inlet of the core which was illustrated by a continuous increase in differential pressure across the core and the first section after several pore volume was injected, interestingly enough is that experimental effluent showed nanoparticles recovery till the end of the experiment. The amount of SNPs retained was estimated to be around 408.81 ± 48.05 µg/gr rock. When the injectivity test was conducted at a high flow rate of 2.5 cm^3/min, the differential pressure dropped fast after injecting 3.00 ± 0.02 PV of brine, and the average pressure at this stage was very much close to that in polymer injectivity test (Test 1). It can be concluded that attraction forces that led to adsorption of silica nanoparticles are weaker than those for polymer since the adsorption amount of the polymer is much higher than the adsorption amount of SNPs.

- Hybrid solution after adsorption test resulted in mobility reduction *RF* of 0.82 ± 0.05, which is slightly higher than what it is found during the polymer adsorption test 0.73± 0.02.

- Although the same concentration of SNPs was used in both Test (2, 3), different behaviors were observed. SNPs in Test 2 caused clogging and high-pressure drop, while in Test 3, no clogging was formed. That shows the influence of polymer to solve the previous problem;

clogging, and also the role of incorporated nanoparticles to improve the polymer viscosity. A possible explanation is that the thermal degradation of PAM-98 at high temperature and high salinity was improved in the presence of SNPs. Underlying mechanisms can be either due to the ability of SNPs to facilitate the cross-links between the polymer inter-chains or due to chemical covalent bonds between the cations of the salts and the oxygen atoms on the surface of SNPs.

- From the effluent analysis, less amount of polymer and SNPs were adsorbed in Test 3. It was found that amount of polymer and SNPs adsorbed on the rock in hybrid dispersion flooding was 59.75 ± 7.10 µg/gr rock and 377.36 ± 56.35 µg/gr rock, respectively.
- To investigate the ability of hybrid solution in improving oil recovery, two-phase core flood experiments were conducted using different model oil; n-hexadecane, and Ondina shell oil, see Appendix C, D and E. However, these experiments did not show any improvement in oil recovery after flooding with Hybrid dispersion at the operating conditions.

Based on the observation and experience gained during this study, the following points can be recommended:

- Re-conduct the experiment using silica nanoparticles with concentration 5,000 mg/L again, but for a longer time to observe the changes in differential pressure and the slope of the profile.

- Hydrophobically modified polyacrylamide behaves differently from hydrolyzed polyacrylamide under harsh conditions of temperature and salinity; therefore, it will be of great interest to study the behaviour of this polymer under different salinity.

- Conduct rheological measurements for silica nanoparticles at different concentrations from one side and for the combination of polymer and SNPs from another side to understand their rheological behaviour and select the best combination for oil recovery improvement.

- Re-evaluate the performance of the hybrid solution as a tertiary method using rocks with a different range of permeabilities. Better to not use Ondina shell oil if the viscosity of the hybrid solution is less than Ondina oil because theoretically, no improvement can be achieved in the mobility ratio due to high viscosity contrast.

- Conduct two-phase experiments, where PAM-98, SNPs and Hybrid dispersion are injected separately as secondary recovery method and compare the cumulative oil production and final oil recovery, water cut, and breakthrough of these chemicals with water flooding as a base case to gain better insight on the performance of these chemicals.

Appendices

A

Tracer potassium Iodide analysis of effluent for single-phase experiments

All adsorption tests conducted in single phase experiments used potassium iodide of 1 wt% concentration as a tracer. The collected effluents were analyzed using *LKB Ultraspec II UV/Visible 4050 spectrophotometer* device ***Figure A.1***. In order to measure the concentration of KI in the effluents, the samples were diluted around 500 times to be within the range of calibration standards.

After that, the measurements start with preparing three cuvettes of standards solutions (0 – 10 – 20 mg/L KI) and setting the device at a wavelength of 226 nm. Each cuvette of standard solution is placed in the cuvette holder, the cleanliness of the inner and outer surface of transparent cuvette must be checked to ensure good quality of the measurements. When the reading signal for (0) mg/L standard solution is stable, the "Zero button" is pressed. Another standard solution is then placed, and the value of ABS is written down to construct the calibration curve.

The process is repeated for diluted samples and this includes the original sample, which is measured three times to obtain the average value. The absorbance is converted into concentration using the linear calibration curve. Tracer concentration in the injected sample is used as a reference since it represents the maximum boundary of potassium iodide.

Figure A.1. Photograph of spectrophotometer device (LKB Ultraspec II UV/Visible 4050)

B

TOC device measurements

Different solutions at the different concentrations used in this project, such as polymer with concentration 500 mg/L and hybrid solution (polymer 500 mg/L and silica-nanofluid 5,000 mg/L). The effluent of the experiments collected at a particular time interval 40 min with flow rate 0.25 cm^3/min is analyzed for the total organic carbon using TOC analyzer; TOC-V CPH/ CPN, Shimadzu (***Figure B.1***). The apparatus consists of several internal components, e.g., vertical combustion tube packed with catalyst, humidifier, TOC furnace, syringe injector, halogen scrubber, and a non-dispersive infrared detector. On the other hand, it is also connected with external elements such as nitrogen cylinder and data processor(computer).

The TOC analyzer is calibrated to measure the maximum concentration of 50 mg/L; therefore, the samples are diluted before measurement with dilution factor about 20, taking into consideration that initial samples weight was 1.5 gr. Afterward, the diluted samples are poured into a glass vial and acidified using a small amount of hydrochloric acid 1.6 of Hydrochloride (HCL). When the injection system injects the samples into the combustion tube, the carbon material is oxidized or decomposes to create carbon dioxide. Next, carrier gas which carries the combustion products from the combustion tube is cooled and dehumidified in the dehumidifier and then passes via halogen scrubber into samples cell of NDID where carbon dioxide is detected. The analog signal of the detector forms a peak and the data processor calculates the peak area. To measure the TOC content of diluted samples, the relation between TOC concentration and peak area (calibrated curve) is established using standard samples. The TOC content measured for the original polymer solution at the injected concentration used as a reference to convert the TOC content measurements of effluents into the polymer concentration.

Figure B.1. Total organic carbon analyzer $TOC - V_{CPH}$ Shimadzu

C

Two-phase experiment using viscous oil – Ondina 3

Two-phase experiment using Ondina Shell oil is conducted according to specific sequence tabulated in Table 3.4. The results of primary drainage and water flooding are shown in Table C.1. Initial oil saturation appears to be high (88 %) due to high oil viscosity compared to brine; nevertheless, residual oil saturation after 5 PV of water flood is around (45%). This can be attributed to a high mobility ratio which does not favor oil displacement in stable conditions.

Table C.1. Summary of the results of two-phase core flood

Process	Parameters	
Oil Saturation	Oil breakthrough at pore volume (-)	0.81 ± 0.02
	Total water produced, Wp (cm^3)	107.5 ± 2.00
	Dead volume (cm^3)	21.00 ± 2.00
	Oil initially in place, OIIP (cm^3)	86.5 ± 2.80
	Initial oil saturation, S_{oi} (%)	80.00 ± 5
	Connate water saturation, S_{wc} (%)	20.00 ± 0.05
	Oil effective permeability, k_o (mD)	1615.08 ± 87.00
	Oil relative permeability, k_{ro}(-)	0.53 ± 0.04
	Oil viscosity at 70 ℃, μ_o (mPa.s)	15.95 ± 0.10
	Oil mobility, λ_o	0.03 ± 0.01
Waterflood	water breakthrough at pore volume (-)	0.33 ± 0.02
	Total oil produced, Wo (cm^3)	56.45 ± 3.00
	Dead volume(cm^3)	18.70 ± 2.00
	Residual oil saturation, S_{or_wF}(%)	45.14 ± 0.03
	Recovery factor, R_{f_wf} (%)	43.64 ± 0.11
	Water effective permeability, k_w(mD)	295.48 ± 18
	Water relative permeability, k_{rw} (-)	0.10 ± 0.01
	Water viscosity at 70 ℃, μ_w (mPa.s)	0.65 ± 0.03
	water mobility, λ_w	0.15 ± 0.02
	Mobility ration $M_{w/o}$ (-)	5.0 ± 1.8

Figure C.1 shows total pressure drop recorded over the core when the oil phase is injected, and it also shows oil cut and water cut associated with this process. It can be observed that water cut equals unity at the start of the process until oil breaks through; the oil phase exits the core. After the breakthrough, only a small amount of water will be produced. It can also be attributed to the high viscosity of the oil, which can push and sweep a large amount of water efficiently, and after

breakthrough two-phase flow starts and little amount of water will be drained with oil. It is worth to mention that changing flow rate can create new dynamic forces which can either increase or decrease the amount of produced water.

Figure C.2 shows the differential pressure generated from waterflood. The pressure drop value is around 55 m Bar with a flow rate of 0.25 cm^3/min, and this value is much lower than the oil pressure drop profile. The reason is high viscosity of oil which leads to higher flow friction than water. Spikes and fluctuation can be observed during waterflood due to the performance of the water injection pump. Figure C.3 shows cumulative oil production. In the beginning, oil production increases linearly at a high slope and then decreases slowly because of two-phase production.

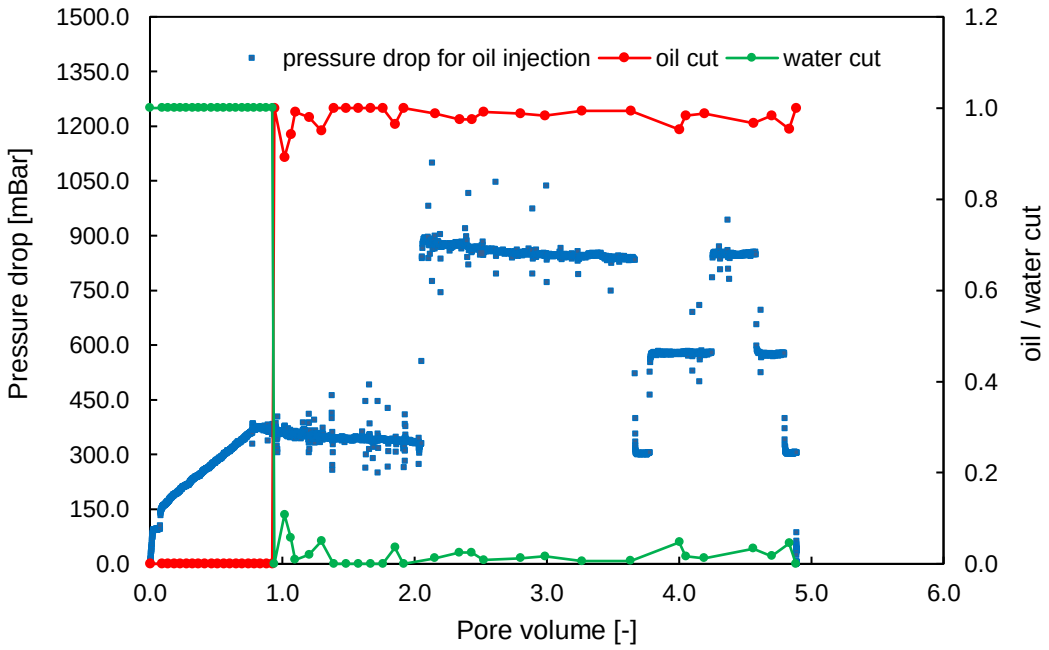

Figure C.1. Total pressure drop profile during oil saturation(drainage), Ondina3

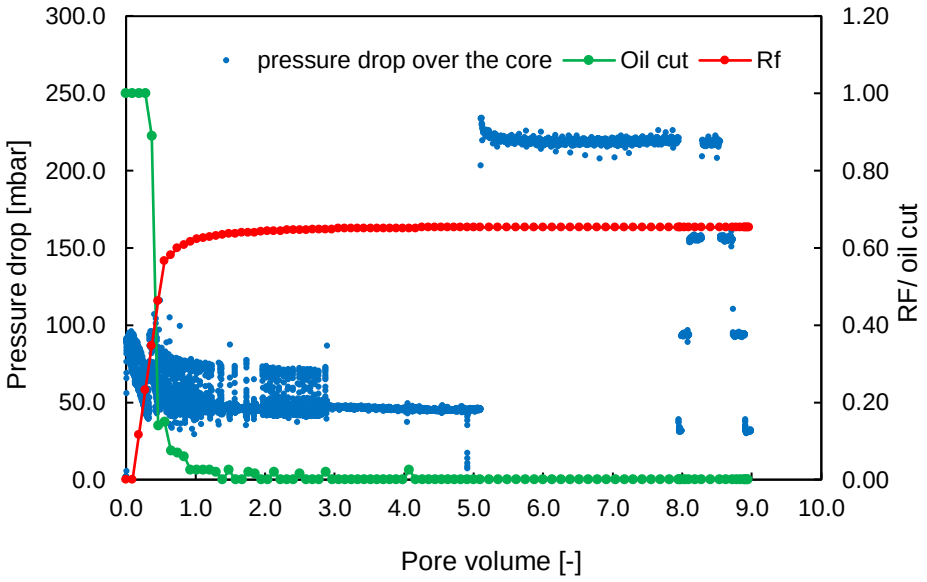

Figure C.2. Total pressure drop profile during water flooding (forced imbibition), Ondina3

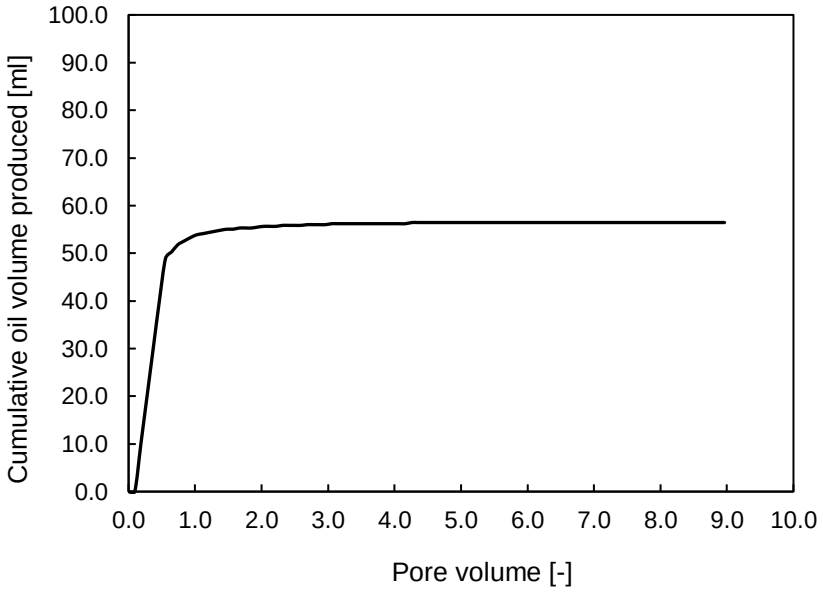

Figure C.3. Cumulative viscous oil production produced by waterflood, Ondina3

D

Two-phase experiment using light oil – N hexadecane

Table D.1. Summary of 2 phase core flood (Test4)

Process	Parameters	
Oil Saturation	Oil breakthrough at pore volume (-)	0.67± 0.02
	Total water produced, Wp (cm^3)	89.00± 2.00
	Dead volume (cm^3)	17.00± 2.00
	Oil initially in place, OIIP (cm^3)	72.00± 2.80
	Initial oil saturation, S_{oi} (%)	66.00± 5
	Connate water saturation, S_{wc} (%)	34.00± 5
	Oil effective permeability, k_o (mD)	1196.28± 64
	Oil relative permeability, k_{ro}(-)	0.45± 0.04
	Oil viscosity at 70 ℃, μ_o (mPa.s)	1.32± 0.01
	Oil mobility, λ_o	0.35± 0.03
Waterflood	water breakthrough at pore volume (-)	0.30± 0.02
	Total oil produced, Wp (cm^3)	41.90± 3.00
	Dead volume(cm^3)	9.50± 2.00
	Residual oil saturation, S_{or_wF}(%)	36.65 ± 5.00
	Recovery factor, R_{f_wf} (%)	45± 5.00
	Water effective permeability, k_w(mD)	437.02± 50
	Water relative permeability, k_{rw} (-)	0.16± 0.02
	Water viscosity at 70 ℃, μ_w (mPa.s)	0.65± 0.03
	water mobility, λ_w	0.25± 0.03
	Mobility ration $M_{w/o}$ (-)	0.71 ± 0.02

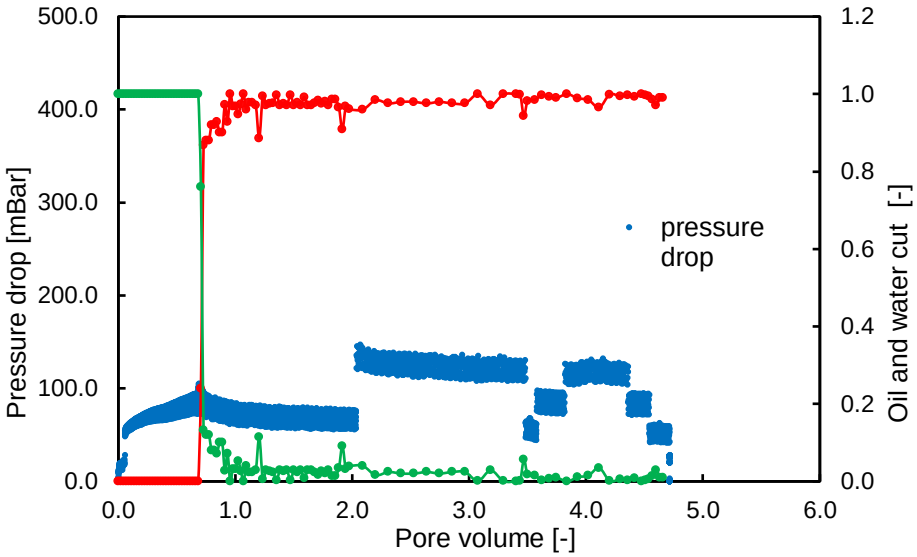

Figure D.1. The total pressure drop profile during oil saturation(drainage), (red) is oil cut, and (olive green) is water cut.

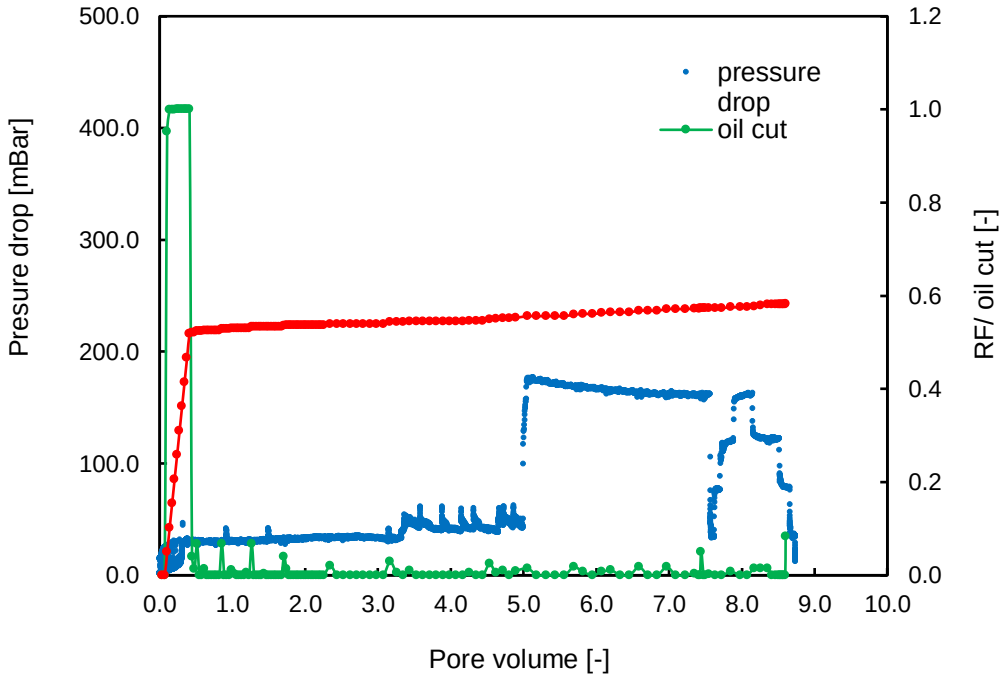

Figure D.2. Total pressure drop profile during water flooding (drainage), (red) is oil cut, and (olive green) is water cut.

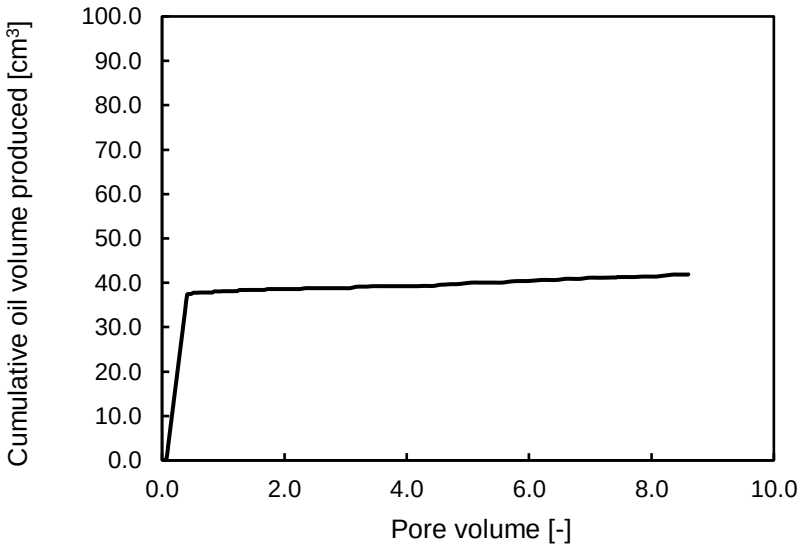

Figure D.3. Cumulative light oil production produced by water flooding

E

Two-phase experiment using viscous oil – Ondina 1

Table E.1. Summary of 2 phase core flood (Ondina1)

Process	Parameters	
Oil Saturation	Oil breakthrough at pore volume (-)	0.82± 0.02
	Total water produced, Wp (cm^3)	107.64 ± 2.00
	Dead volume (cm^3)	17.00 ± 2.00
	Oil initially in place, OIIP (cm^3)	90.64 ± 2.80
	Initial oil saturation, S_{oi} (%)	83.91 ± 5.00
	Connate water saturation, S_{wc} (%)	16.09 ± 5.00
	Oil effective permeability, k_o (mD)	1615.04 ± 87.00
	Oil relative permeability, k_{ro}(-)	0.57 ± 0.05
	Oil viscosity at 70 ℃, μ_o (mPa.s)	15.85 ± 0.10
	Oil mobility, λ_o	0.04 ± 0.01
Waterflood	water breakthrough at pore volume (-)	0.31 ± 0.02
	Total oil produced, Wp (cm^3)	50.24 ± 3.00
	Dead volume(cm^3)	9.33 ± 2.00
	Residual oil saturation, S_{or_wF}(%)	46.04 ± 5.00
	Recovery factor, R_{f_wf} (%)	45.13 ± 4.00
	Water effective permeability, k_w(mD)	273.01± 16.88
	Water relative permeability, k_{rw} (-)	0.1 ± 0.01
	water viscosity at 70 ℃, μ_w (mPa.s)	0.65 ± 0.03
	water mobility, λ_w	0.15± 0.01
	Mobility ration $M_{w/o}$	3.5 ± 0.97

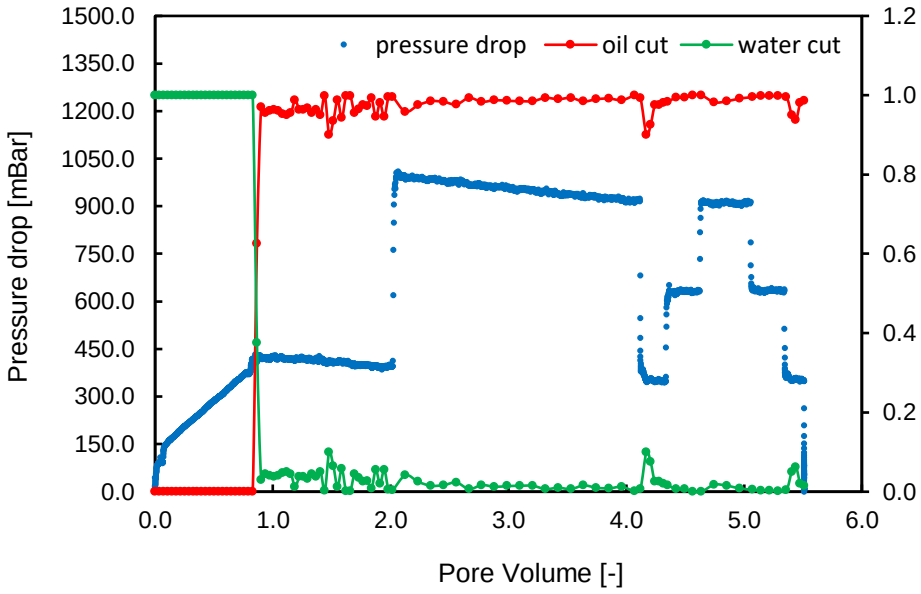

Figure E.1. Total pressure drop profile during oil saturation(drainage)

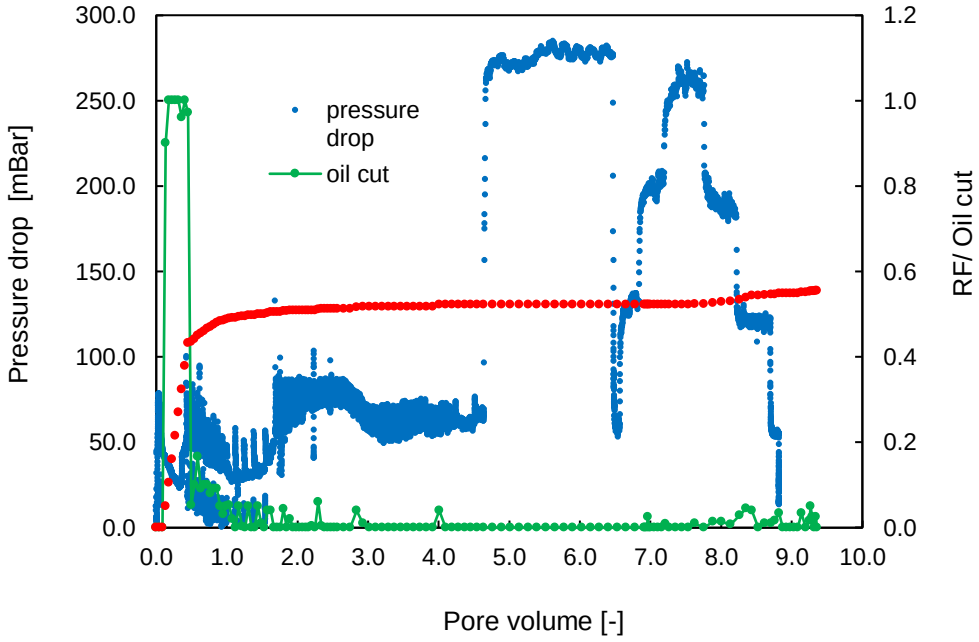

Figure E.2. Total pressure drop profile during water saturation (forced imbibition)

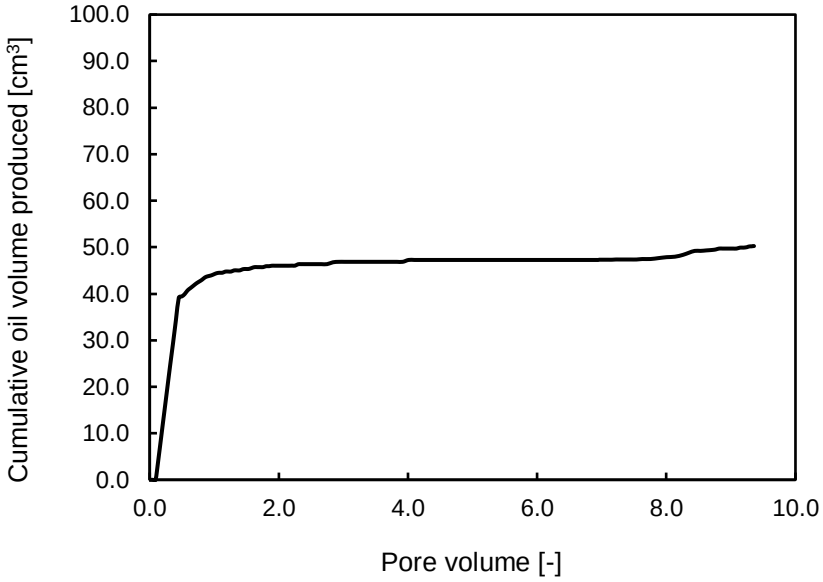

Figure E.3. Cumulative viscous oil production produced by water flooding

F

Microfluidic Experiment

The objective of these experiments is to investigate the potential of the hybrid solution as a tertiary method to improve the oil recovery factor and study on a microscopic level to what extend new chemicals are able to remove oil from narrow pores by evaluating their behaviour in comparison with waterflood (secondary recovery) and another different solution such as polymer solution (tertiary recovery). With the use of a micromodel, supplied by Micronit, and high-speed camera images of fluid propagation are captured, and pressure data is recorded. These data were then processed mainly ImageJ software. Micromodels used in this study are held within a chip holder and can be described as a physical network etched onto the surface of a glass plate. This plate was then wrapped with another flat plate to seal the channels. This assembly formed a two-dimensional path through which flow behaviour can be visually observed and oil recovery can be assessed.

F.1 Experimental setup

Figure F.1 and **Figure F.2** show a scheme and photograph of the experimental setup used for conducting the microfluidic experiment, respectively. As indicated in the scheme, a chemically etched transparent micro-flow model manufactured by Micronit company is used to visualize the flow behavior. The chip is installed inside a unique chip holder. The length of the chip including and excluding the sidebar channels, is 19.72 cm, 17.782 cm, respectively, and the width of the chip is 9.38 cm. The average depth of the channels is about 20 microns, and rock pore volume provided by the factory was 2.3 μl. The injection system for micro-model experiments consists of a Harvard pump to inject the fluid using BD plastic syringe with different capacity volumes (5 or 3) ml. Two pressure transducers PT1, PT2 with range (0-500) mbar are installed to the inlet and the outlet of the micro-flow model to record the pressure difference across the chip. A high-speed video camera mounted on the optical microscopy (Leica) was used to capture images at the pore-scale level, and it was linked to a computer running Midas 2.0 software, which helped to adjust parameters related to the camera. At the inlet of the system, there is a three-way valve to get rid of any air bubbles that inevitably entered the tubing while changing syringes. A wooden box was constructed to provide some degree of flexibility to slide the chip holder under the microscope to optimize the visualization of specific spots during the study.

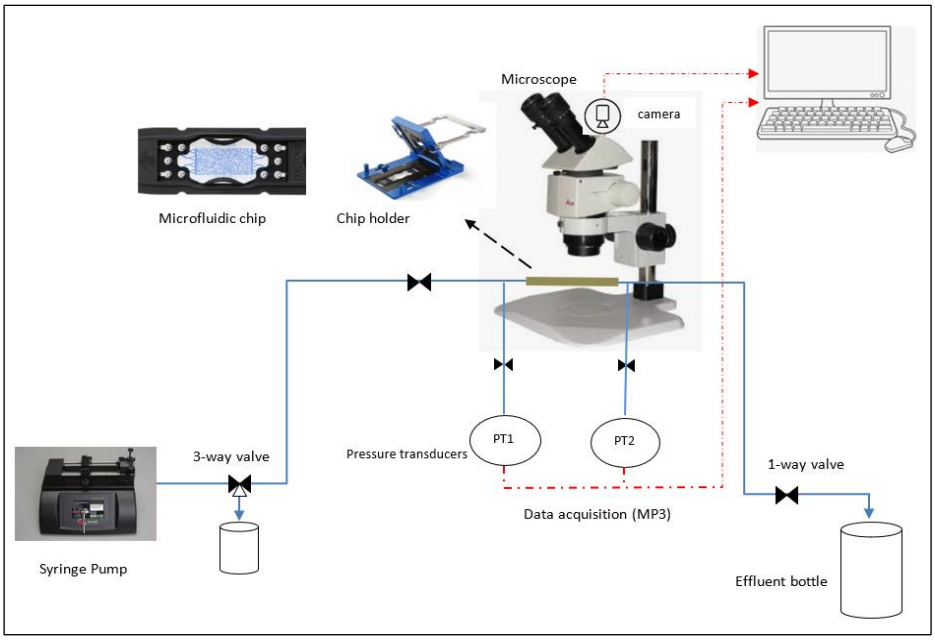

Figure F.1. Schematic diagram of the microfluidic experiment

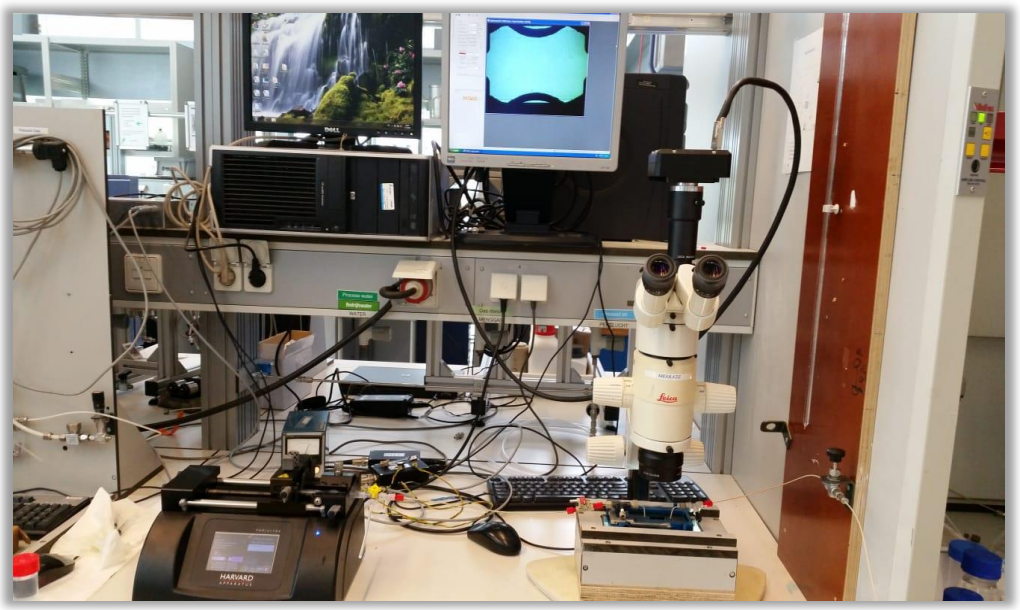

Figure F.2. Photo of microfluidic experiment

F.2 Chemical materials

Microfluid experiments were conducted at different conditions than core floods. While core flood experiments were performed at a T= 70 °C and used model oil such as Ondina shell oil and n-hexadecane, the microfluidic tests are carried out at room temperature where crude oil was used. The oil has a dark brown color and is very visible when injected in the microchip. A rheology study was done to find the viscosity of the oil using a rheometer, oil had a viscosity of 44 ± 0.1 mPa.s at

temperature 23˚C. For chip saturation and waterflood, brine with two different salinity is used. Experiment with the hybrid solution used a brine of total salinity of 200 g/L, while experiment with only polymer solution used a brine of total salinity of 200 g/L, which contained 2% of divalent calcium ions Ca^{++}. The brine viscosity at 23˚C is 1.9 ± 0.1 mPa.s. In addition, a different type of polymers was used, such as polyacrylamide PAM-100 and hydrophobically modified polymer PAM-98. PAM-100 was used with concentration 5 g/l as tertiary recovery, whereas PAM-98 was used in combination with silica nanoparticles to form a hybrid solution.

Table F.1. Chemical materials used after water flood and total salinity

Chemical materials	Test 1 (mg/L)	Test2(mg/L)
PAM 100	-	5,000
PAM98	500	-
Silica NPs	5,000	-
Salinity TDS (Na^{+}, Ca^{++})	200,000 (1.5% Ca^{+2})	250,000(2% Ca^{+2})

F.3 Results and discussion

The results are obtained by Rens van der Vleuten during his work on his bachelor thesis under my daily supervision.

F.3.1 Hybrid solution (PAM-98,500mg/L+ silica nanoparticles, 5000 mg/L)

- **Oil saturation**

  After saturating the chip with enough pore volume of brine, a picture was taken to be used as a mask, so pictures of subsequent processes can be compared with (***Figure F.3***).

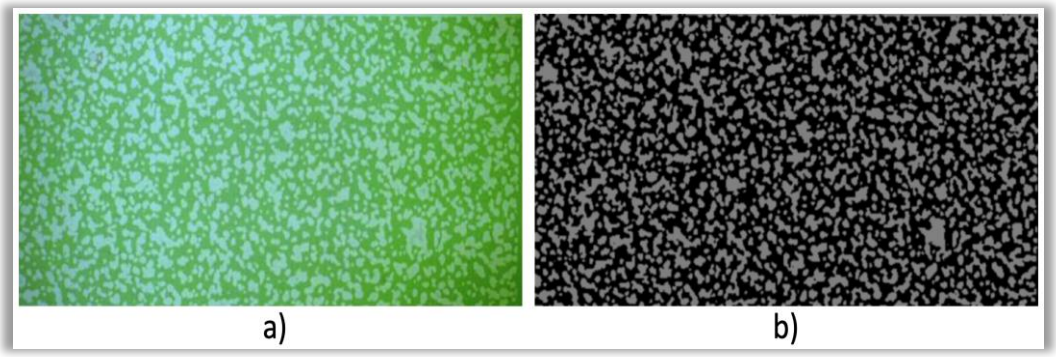

Figure F.3. a) Picture of microchip saturated with colored demineralized water. b) Processed picture - the mask (grey = grain, black = pore space)

Figure F.4 shows the gradual propagation of crude oil through the micromodel where the direction of all injected materials in this experiment is from left to right. The first raw pictures represent the actual

microscopic pictures took using a high-speed camera, while the pictures in the second raw are the processed pictures using Image J software.

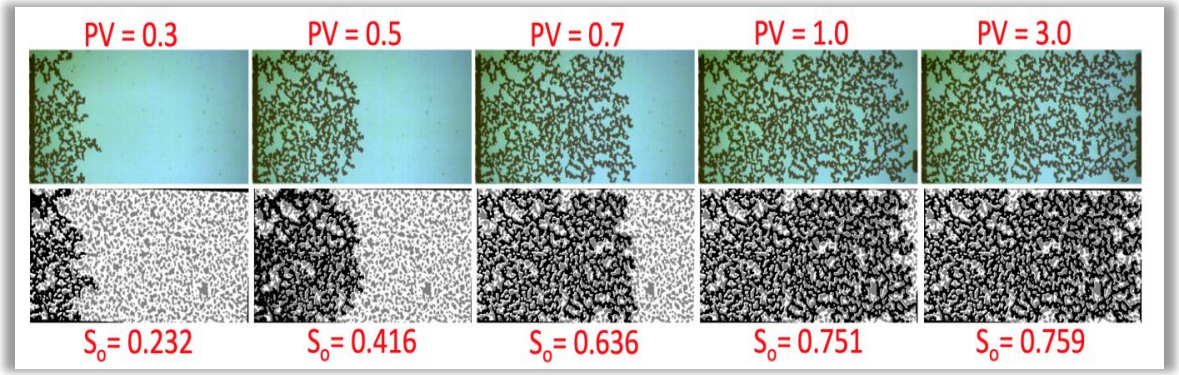

Figure F.4. Propagation of oil in micromodel

It can be observed that oil saturation after one pore volume has almost reached the maximum saturation value $S_o = 0.75$, since saturation after 3 pore volume is only increased 1 %. Comparing oil saturation picture with the mask (brine saturation picture), the unsaturated area can be spotted (***Figure F.5***)

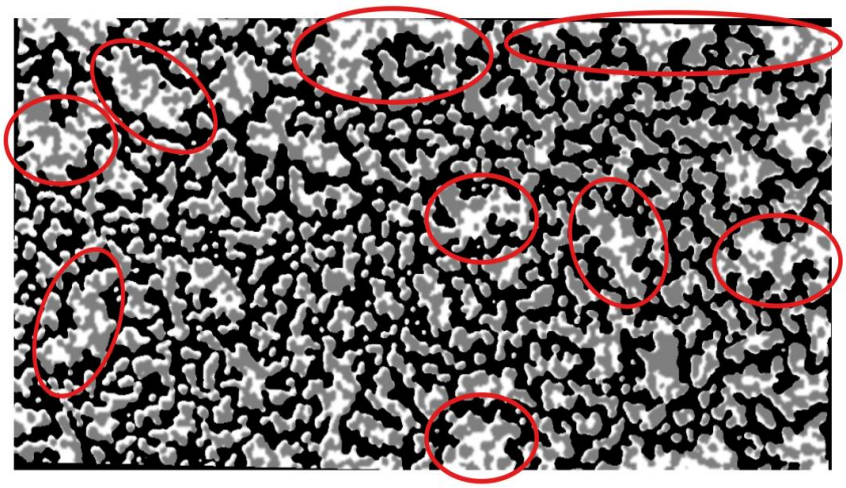

Figure F.5. shows unsaturated chip area of oil

Figure F.5 shows that the upper half of the chip is not being saturated as well as some other area. This can be explained due to the way the inlet of the chip is constructed and grain distribution.

- **Brine flooding:**

The oil saturation process is followed by water flooding, which is a secondary recovery method in the actual reservoir cycle, however, it is considered a primary recovery method in laboratory work. **Figure F.6** clearly shows how waterfront propagates inside the chip, and the amount of oil remained behind due to bypassing and capillary pressure. Remaining oil saturation hardly experiences any change after 1 PV.

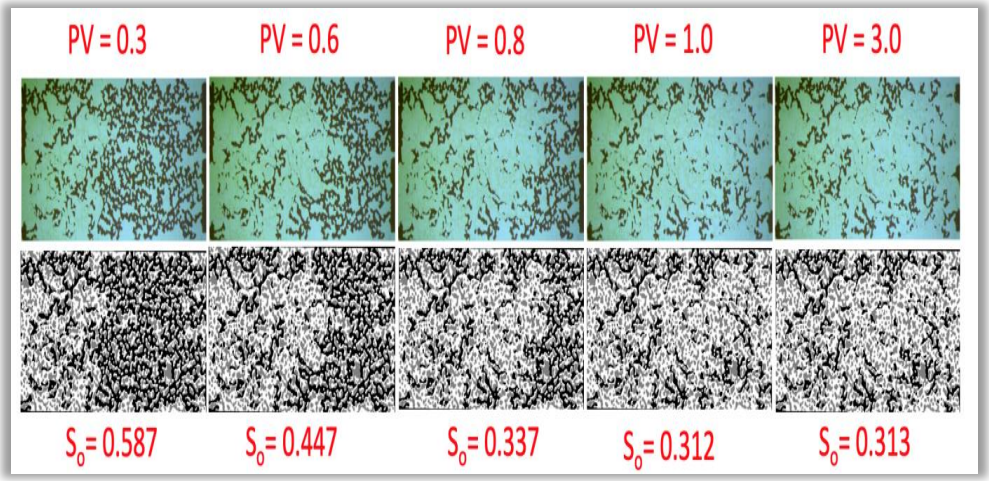

Figure F.6. Water flood propagation and remaining oil distribution at different pore volume

The viscosity of the water is much less than that of crude oil, therefore the mobility ration is unfavored. ***Figure F.7*** shows the amount of oil left behind after injecting 3 PV at a very low flow rate of 37.5 nl /min and similar to primary drainage, certain parts are affected less than others.

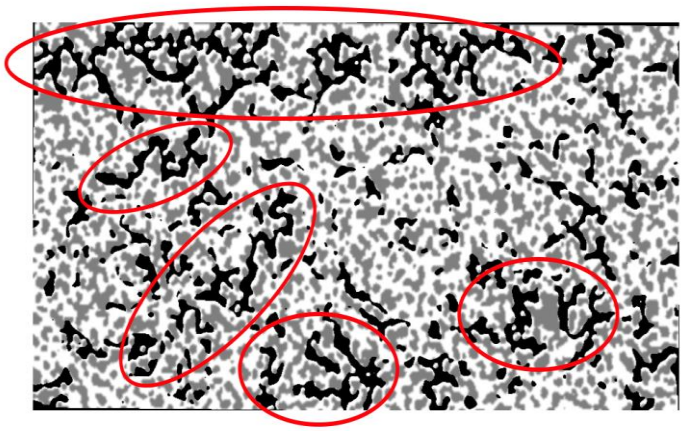

Figure F.7. Remaining oil saturation after injecting 3 PV of brine

Waterflooding was less effective at the top boundary of the chip and at some spots in the lower part. To interpret this problem, another look at the inlet channels was needed. ***Figure F.8*** shows the possible reason. The green box marks the inlet channel through which the brine flushed the microchip. The red box shows the top channels not being flushed, meaning no brine flow.

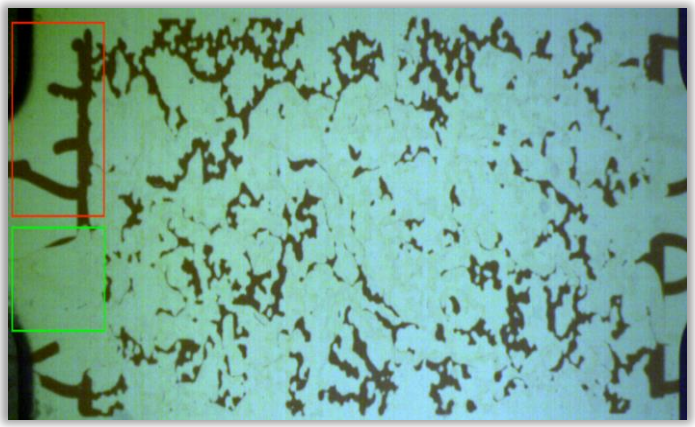

Figure F.8. Part of inlet distributary channel is blocked for water to enter the micromodel

- **Hybrid solution flooding:**

Evaluating the ability of (polymer – nanoparticles) solution in displacing oil from narrow channels compared to water flooding from one hand and to polymer solution with concentration 5,000 mg/L from another hand, is the main objective of the microfluid experiment in this study. Injecting hybrid solution after waterflood is accompanied by a challenge in determining the entry time of the solution into the chip visually since both brine and hybrid solution are apparently transparent. Nevertheless, entry time can be estimated to good extend using calculated dead volume and the recorded inlet pressure data, therefore care should be taken in selecting pressure transmitters measure range and ensure their reliability.

Figure F.9 shows the processed microscopic picture as a result of injecting 3 PV of the hybrid solution after water flooding.

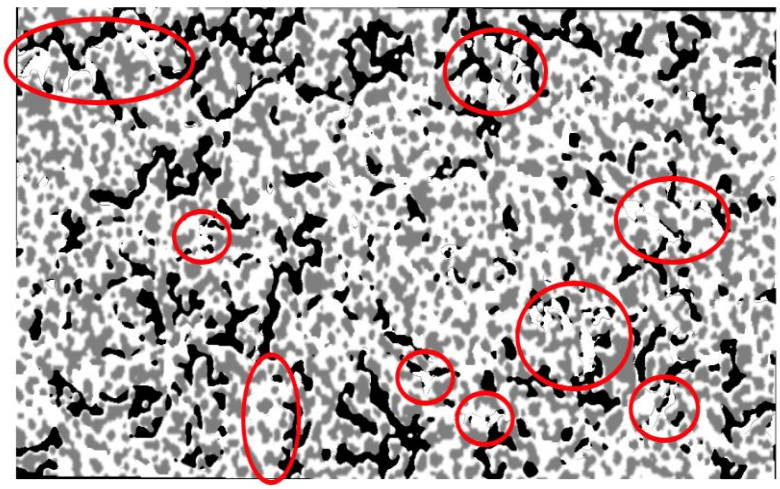

Figure F.9. Remaining oil distribution in the micromodel after Hybrid flooding

The red circles indicate the areas where extra oil was recovered after injecting the hybrid solution. Increasing sweep area by the hybrid solution is mainly observed in the lower right part and can be attributed to combined factors such as high viscosity of the solution which results in improving the mobility ratio of displacing fluid and potentially to disjoining pressure mechanism ***Figure 2.5***. On the other hand, it was found that the hybrid solution is flying through more inlet channels than waterflood, and this could be due to the sticking nature of nanoparticles solution.

Another type of flood was conducted in Test 2 in order to investigate the effectiveness of a hybrid solution in comparison with the polyacrylamide solution at a concentration of 5,000 mg/L. The result is illustrated in ***Figure F.10***, ***Figure F.11*** which shows the remaining oil after waterflood and subsequent polymer flood. The result is interesting since less area of micromodel was swept after polymer flooding although the viscosity of polymer solution is higher than the solution in Test 1.

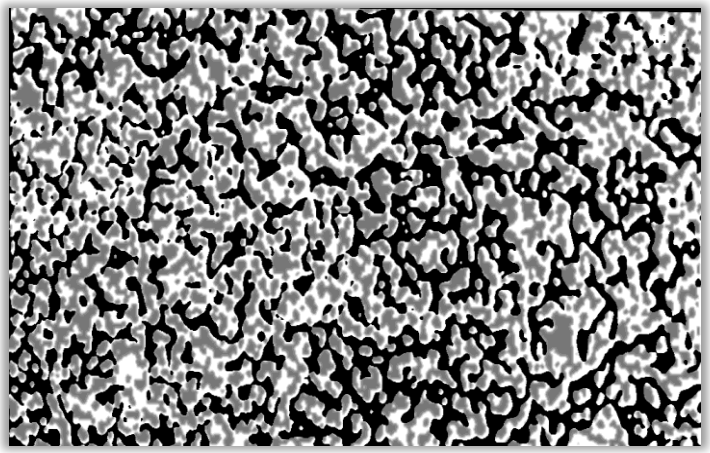

Figure F.10. Remaining oil saturation after injecting 3 PV of brine (Test2)

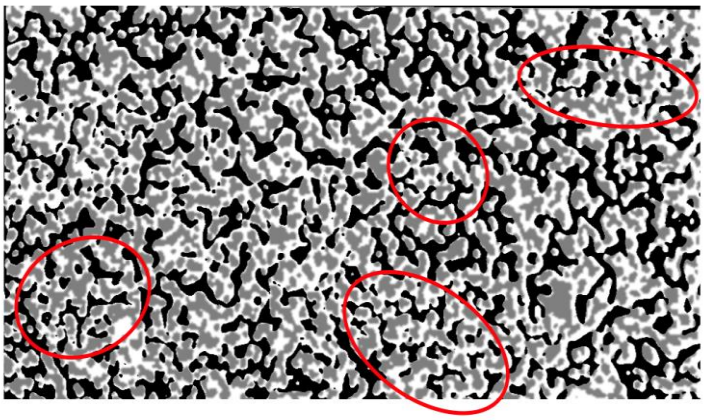

Figure F.11. Remaining oil inside microchip after polymer flooding (Test 2)

Table F.2. Results comparison between the two experiments

	Test 1	Test 2
S_{oi} (%)	76	76
S_{or_wF} (%)	31	58
R_{f_wf} (%)	59	24
S_{or_HS} (%)	27	54
R_{f_HS} (%)	64	29
$\Delta R_{f(wf,HS)}$(%)	5	5

F.4 Summary of microfluid experiments

During microfluidic experiments, two different tests are conducted. The first test is done using hybrid dispersion (PAM98+silica NPs) and the second test is performed using polymer solution PAM-100. Both tests illustrated that oil saturation inside the chip had reached the maximum value almost after 1 PV was injected. However, water flood for each test resulted in different recovery factor due to the fact that water had flown in different paths in the inlet distributary channels; in Test 1 brine had entered the chip after it occupied most of the inlet paths, which was not the case in Test 2, probably due to some blockage owned to salt precipitation.

Both solutions increased the recovery factor by 5% after waterflood, nevertheless, the hybrid solution led to the highest ultimate recovery factor 64 % while the polymer solution achieved 29%.

G

References

1. Al-Shakry, B., T. Skauge, B. S. Shiran and A. Skauge (2018). "Polymer Injectivity: Investigation of Mechanical Degradation of EOR Polymers Using In-Situ Rheology."
2. Anderson, W. (1986). "Wettability literature survey-part 2: Wettability measurement." Journal of petroleum technology **38**(11): 1,246-241,262.
3. Argillier, J.-F., A. Audibert, J. Lecourtier, M. Moan and L. Rousseau (1996). "Solution and adsorption properties of hydrophobically associating water-soluble polyacrylamides." Colloids and Surfaces A: Physicochemical and Engineering Aspects **113**(3): 247-257.
4. Aubry, T. and M. Moan (1998). "Rheological behavior of a hydrophobically associating water soluble polymer." Journal of Rheology **38**(6): 1681.
5. Baez, J., M. P. Ruiz, J. Faria, J. H. Harwell, B. Shiau and D. E. Resasco (2012). Stabilization of interfacially-active-nanohybrids/polymer suspensions and transport through porous media. SPE Improved Oil Recovery Symposium, Society of Petroleum Engineers.
6. Bradford, S. A. and S. Torkzaban (2008). "Colloid transport and retention in unsaturated porous media: A review of interface-, collector-, and pore-scale processes and models." Vadose Zone Journal **7**(2): 667-681.
7. Chauveteau, G. and N. Kohler (1974). Polymer flooding: The essential elements for laboratory evaluation. Spe improved oil recovery symposium, Society of Petroleum Engineers.
8. Chengara, A., A. D. Nikolov, D. T. Wasan, A. Trokhymchuk and D. Henderson (2004). "Spreading of nanofluids driven by the structural disjoining pressure gradient." Journal of colloid and interface science **280**(1): 192-201.
9. Churaev, N. (2003). "Surface forces in wetting films." Colloid Journal **65**(3): 263-274.
10. Craig, F. F. (1971). The reservoir engineering aspects of waterflooding, HL Doherty Memorial Fund of AIME New York.
11. Darcy, H. P. G. (1856). Les Fontaines publiques de la ville de Dijon. Exposition et application des principes à suivre et des formules à employer dans les questions de distribution d'eau, etc, V. Dalamont.
12. Dawson, R. and R. B. Lantz (1972). "Inaccessible pore volume in polymer flooding." Society of Petroleum Engineers Journal **12**(05): 448-452.
13. Ersenkal, D. A., A. Ziylan, N. H. Ince, H. Y. Acar, M. Demirer and N. K. Copty (2011). "Impact of dilution on the transport of poly (acrylic acid) supported magnetite nanoparticles in porous media." Journal of contaminant hydrology **126**(3-4): 248-257.
14. Green, D. W. and G. P. Willhite (1998). Enhanced oil recovery, Henry L. Doherty Memorial Fund of AIME, Society of Petroleum Engineers ….
15. Hendraningrat, L. and O. Torsæter (2014). "Effects of the initial rock wettability on silica-based nanofluid-enhanced oil recovery processes at reservoir temperatures." Energy & Fuels **28**(10): 6228-6241.

16. Jamshidi, N. and M. Khodadadi (2012). "Experimental investigation on the viscosity of nanofluids." International Journal of Engineering **25**(3): 201-210.
17. Jouenne, S. and G. Heurteux (2017). Flow of polymer solutions through porous media-prediction of mobility reduction from ex-situ measurements of elasticity. IOR 2017-19th European Symposium on Improved Oil Recovery.
18. Kondiparty, K., A. D. Nikolov, D. Wasan and K.-L. Liu (2012). "Dynamic spreading of nanofluids on solids. Part I: experimental." Langmuir **28**(41): 14618-14623.
19. Miranda, C. R., L. S. d. Lara and B. C. Tonetto (2012). Stability and mobility of functionalized silica nanoparticles for enhanced oil recovery applications. SPE International Oilfield Nanotechnology Conference and Exhibition, Society of Petroleum Engineers.
20. Niu, Y., O. Jian, Z. Zhu, G. Wang and G. Sun (2001). Research on hydrophobically associating water-soluble polymer used for EOR. SPE International Symposium on Oilfield Chemistry, Society of Petroleum Engineers.
21. Peksa, A. E., K.-H. A. Wolf and P. L. Zitha (2015). "Bentheimer sandstone revisited for experimental purposes." Marine and Petroleum Geology **67**: 701-719.
22. Roustaei, A., S. Saffarzadeh and M. Mohammadi (2013). "An evaluation of modified silica nanoparticles' efficiency in enhancing oil recovery of light and intermediate oil reservoirs." Egyptian Journal of Petroleum **22**(3): 427-433.
23. Sheng, J. (2010). Modern chemical enhanced oil recovery: theory and practice, Gulf Professional Publishing.
24. Sorbie, K. S. (1991). Polymer-improved oil recovery, Springer Science & Business Media New York.
25. Szabo, M. (1975). "Some aspects of polymer retention in porous media using a C14-tagged hydrolyzed polyacrylamide." Society of Petroleum Engineers Journal **15**(04): 323-337.
26. Taylor, K. and H. Nasr-El-Din (2007). Hydrophobically associating polymers for oil field applications. Canadian International Petroleum Conference, Petroleum Society of Canada.
27. Wang, W., Y. Liu and Y. Gu (2003). "Application of a novel polymer system in chemical enhanced oil recovery (EOR)." Colloid and Polymer Science **281**(11): 1046-1054.
28. Wang, Y., B. Li, X. Xiong, B. Wang and J. Zhang (2010). "Universal scaling description of the strain-softening behavior in the semidilute uncross-linked polyacrylamide-water solution." Soft Matter **6**(14): 3318-3324.
29. Yang, B., J. Mao, J. Zhao, Y. Shao, Y. Zhang, Z. Zhang and Q. Lu (2019). "Improving the Thermal Stability of Hydrophobic Associative Polymer Aqueous Solution Using a "Triple-Protection" Strategy." Polymers **11**(6): 949.
30. Yerramilli, S. (2012). "Analysis of Polymer Injectivity in Porous Media: Experiments and Modelling."
31. Zaitoun, A. and B. Potie (1983). Limiting conditions for the use of hydrolyzed polyacrylamides in brines containing divalent ions. SPE Oilfield and Geothermal Chemistry Symposium, Society of Petroleum Engineers.
32. Zhang, H., A. Nikolov and D. Wasan (2014). "Enhanced oil recovery (EOR) using nanoparticle dispersions: underlying mechanism and imbibition experiments." Energy & Fuels **28**(5): 3002-3009.
33. Zitha, P. L., G. Chauveteau and L. Léger (2001). "Unsteady-state flow of flexible polymers in porous media." Journal of colloid and interface science **234**(2): 269-283.
34. https://www.sigmaaldrich.com/catalog/product/vetec/v900147?lang=en&region=US
35. https://www.b2bcomposites.com/msds/ted/40831.pdf